Standard treatment against paediatric BRAF-V600E glioma promotes senescence and sensitizes tumours to BCL-xL inhibition

Authors

Romain Guiho[1,2*#], Hiba Hamdi[1#], Grace Cooksley[1], Timoty H. Chang[3], Lei Cao[1,4], Romain Sigaud[5,6], Sophie Bliss[1,7], Ashley Vardon[1,8], Scott Haston[1], Florian Selt[9,10], Akang Leonard Bassey[1], Daniela Kocher[5,6], Ria Kedia[3], Daniel Gharai[1], Jesús Gil[7,11], Olaf Witt[12,13], Till Milde[5,6,12,13], Darren Hargrave[1,14], Paula Alexandre[1], Pratiti Bandopadhayay[3], Juan Pedro Martinez Barbera[1*]

Affiliations

[1] Developmental Biology and Cancer Programme, Birth Defects Research Centre, Great Ormond Street Institute of Child Health, University College London, London, UK.

[2] Nantes Université, Oniris, INSERM, Regenerative Medicine and Skeleton, RMeS, UMR 1229, F-44000 Nantes, France.

[3] Department of Pediatric Oncology, Dana-Farber Cancer/Boston Children's Cancer and Blood Disorders Center, Boston, MA, USA.

[4] Department of Neurosurgery, Beijing Tiantan Hospital, Capital Medical University, Beijing, China.

[5] University Hospital Jena, Department of Pediatrics and Adolescent Medicine, Friedrich Schiller University Jena, Jena, Germany.

[6] Comprehensive Cancer Center Central Germany (CCCG), Jena, Germany.

[7] MRC Laboratory of Medical Sciences (LMS), Du Cane Road, London, W12 0NN, UK.

[8] Institute of Cancer and Genomic Medicine, University of Birmingham, Birmingham, UK.

[9] Clinical Trial Unit (ZIPO), Department of Pediatric Hematology, Oncology, Immunology and Pulmonology, Heidelberg University Hospital, Heidelberg, Germany.

[10] National Center for Tumor Diseases (NCT), Heidelberg, Germany.

© The Author(s) 2026. Published by Oxford University Press on behalf of the Society for Neuro-Oncology.
This is an Open Access article distributed under the terms of the Creative Commons Attribution License (https://creativecommons.org/licenses/by/4.0/), which permits unrestricted reuse, distribution, and reproduction in any medium, provided the original work is properly cited.

ACCEPTED MANUSCRIPT

Downloaded from academic.oup.com/neuro-oncology/advance-article/doi/10.1093/neuonc/noag270/9004423 by Imperial College of Science Technology and Medicine user on 02 November 2026

[11] Institute of Clinical Sciences (ICS), Faculty of Medicine, Imperial College London, Du Cane Road, London W12 0NN, UK.

[12] Hopp Children's Cancer Center Heidelberg (KiTZ), Heidelberg, Germany.

[13] Clinical Cooperation Unit Pediatric Oncology, German Cancer Research Center Heidelberg (DKFZ), Heidelberg, Germany.

[14] Great Ormond Street Hospital NHS Trust, London, United Kingdom.

[#] Equal contributors

Running Title: Senolytics against BRAF-V600E low-grade glioma

*** Corresponding authors:**

Romain Guiho – romain.guiho@univ-nantes.fr, Nantes Université, Oniris, INSERM, Regenerative Medicine and Skeleton, RMeS, UMR 1229, School of dental medicine, 1 place Alexis Ricordeau, 44042 Nantes cedex 1, France.

Prof. JP Martinez-Barbera – j.martinez-barbera@ucl.ac.uk, Developmental Biology and Cancer Programme, Birth Defects Research Centre, Great Ormond Street Institute of Child Health, University College London, London, UK

Total manuscript word count (including abstract, text, references, and figure legends)

8 380

Main text word count (Introduction to discussion)

4 994

Preprint

The manuscript has been deposited on BioRXiv

https://doi.org/10.64898/2026.01.13.698644

ACCEPTED MANUSCRIPT

Downloaded from academic.oup.com/neuro-oncology/advance-article/doi/10.1093/neuonc/noag270/9004423 by Imperial College of Science Technology and Medicine user on 02 November 2026

Abstract

Background. Chemo-, radio-, and targeted therapies can induce a stable growth arrest known as therapy-induced senescence (TIS), which may be therapeutically exploited using senolytic compounds that selectively eliminate senescent cells. Children with BRAF-V600E-driven brain tumours are commonly treated with low-dose chemotherapies and MAPK inhibitors, alone or in combination, often with good initial responses. However, a majority of patients experiences tumour regrowth following treatment withdrawal. Here, we investigate the contribution of TIS to treatment response and relapse, and assess the therapeutic potential of senolytics in preclinical models of paediatric BRAF-V600E glioma.

Methods. Preclinical models of paediatric low-grade glioma were analysed in vitro or following orthotopic transplantation into mice and treated with Dabrafenib, Trametinib, Tovorafenib or Vinblastine. Senescence was assessed using molecular and cytological markers. Sensitivity to senolytic compounds was evaluated using in vitro dose-response assays and in vivo treatment studies.

Results. Trametinib induced a robust senescent phenotype in BT-40 tumours in vivo, characterised by activation of a senescence-associated secretory phenotype and expansion of IBA-1-positive myeloid cells. In vitro, senescence was induced in BT-40 cells following treatment with MAPK inhibitors and Vinblastine, and was similarly observed in H9-derived human neural stem cells expressing BRAF-V600E. Navitoclax was identified as a potent senolytic against senescent BT-40 cells, primarily through inhibition of the anti-apoptotic protein BCL-xL. In vivo, combined Trametinib and Navitoclax treatment ablated senescent tumour cells, significantly reduced tumour regrowth after treatment withdrawal, and improved survival.

Conclusions. These findings demonstrate that Navitoclax enhances Trametinib's anti-tumour efficacy and limits tumour relapse following treatment cessation.

Keywords: BRAF-V600E driven glioma; BT-40; MAPK inhibitors; Navitoclax; senescence

Key Points

- MAPK inhibitors and Vinblastine induce senescence in BRAF-V600E altered cells in vitro
- Senescent BT-40 cells are sensitive to BCL-xL inhibition
- Combination of Trametinib and Navitoclax reduces rebound tumour growth in vivo

ACCEPTED MANUSCRIPT

Downloaded from academic.oup.com/neuro-oncology/advance-article/doi/10.1093/neuonc/noag270/9004423 by Imperial College of Science Technology and Medicine user on 02 November 2026

Importance of the Study

Children with BRAF-V600E activated glioma are frequently treated with MAPK inhibitors (e.g., Dabrafenib, Trametinib) or low dose chemotherapy (e.g., Vinblastine, carboplatin/vincristine) with good responses. However, a majority of patients show tumour regrowth when the treatment is stopped, requiring them to endure prolonged treatment that may impair quality of life, alongside a persistent risk of malignant progression. Our research demonstrates that these therapies induce BT-40 tumour cells to enter a non-proliferative state that shows features of cellular senescence. We identify that senescent tumour cells can be killed using Navitoclax, and potent inhibitor of the anti-apoptotic protein BCL-xL and a well-studied senolytic. We demonstrate that the combination of Trametinib and Navitoclax reduces tumour regrowth after treatment withdrawal. Our research provides a strong rationale supporting the combined use of senolytics with current conventional and targeted therapies against BRAF-V600E mutated brain tumours.

ACCEPTED MANUSCRIPT

Downloaded from academic.oup.com/neuro-oncology/advance-article/doi/10.1093/neuonc/noag270/9004423 by Imperial College of Science Technology and Medicine user on 02 November 2026

Introduction

Brain tumours represent the most prevalent solid malignancies in children and the leading cause of cancer-related mortality in this population, with low-grade gliomas (LGG) accounting for 30–40% of central nervous system (CNS) tumours[1]. Clinical manifestations vary widely in LGG, primarily due to the compressive effects of the tumour on adjacent brain tissue or cerebrospinal fluid flow obstruction, often presenting with seizures, headaches, or alterations in cognition and behaviour. These tumours typically exhibit slow progression, limited invasiveness, and a low Ki-67 proliferation index[2,3].

Genomic analyses have identified *KIAA1549::BRAF* fusions as the most frequent alteration in paediatric pilocytic astrocytomas, whereas BRAF-V600E mutations are common in gangliogliomas and more aggressive brain tumours such as diffuse astrocytomas, glioblastomas and pleomorphic xanthoastrocytomas[4–9]. Treatment strategies depend on resectability and may involve surgery, MAPK-pathway inhibitors (MAPKi)[10], radiotherapy, or chemotherapy. While the combination of carboplatin and vincristine remains a standard regimen, vinblastine monotherapy has established an emerging role as an effective first-line treatment with a favourable toxicity profile[11]. Initial preclinical studies using the BT-40 cell line, which was isolated from a patient with pleomorphic xanthoastrocytoma (PXA) harbouring the BRAF-V600E mutation and *CDKN2A/B* deletion, demonstrated the efficacy of MEK inhibitors against these tumours[12,13]. Subsequent clinical trials confirmed these findings, and recent investigations have further validated the use of combined BRAF and MEK inhibition, exemplified by dabrafenib and trametinib, against both fusion-positive and BRAF-mutant tumours, leading to regulatory approval for paediatric BRAF-V600E-driven gliomas[14–17]. Despite the good responses elicited by these MAPKi, a majority of patients shows tumour regrowth following discontinuation of treatment[14,18]. Although the reasons underlying this rebound growth remain unknown, rapid reactivation of the MAPK pathway has been observed in vitro, suggesting an intrinsic rebound mechanism within tumour cells. Additionally, elevated secretion of cytokines that recruit microglia may influence treatment responsiveness and post-therapy tumour regrowth[19].

Senescence represents a cellular defence mechanism triggered by various stressors, including oncogenic signalling, replicative exhaustion, and DNA damage. Once senescence is initiated, cells undergo a stable proliferation arrest, orchestrated by key regulatory pathways such as p53/p21 and p16/RB. Beyond cell cycle exit, senescent cells exhibit non-cell-autonomous effects through the senescence-associated secretory phenotype (SASP). The SASP comprises a diverse array of secreted factors, including pro-inflammatory

ACCEPTED MANUSCRIPT

Downloaded from academic.oup.com/neuro-oncology/advance-article/doi/10.1093/neuonc/noag270/9004423 by Imperial College of Science Technology and Medicine user on 02 November 2026

cytokines/chemokines and growth factors that can influence neighbouring cells and the tumour microenvironment[20,21]. Notably, conventional and targeted cancer therapies, such as radiotherapy, chemotherapy and molecular inhibitors, can promote therapy-induced senescence (TIS) in tumour cells. Residual senescent cells post-treatment may paradoxically facilitate tumour recurrence[22,23]. This can occur through cell-autonomous mechanisms, such as reactivation of proliferation due to p53/p21 or p16/RB pathway inactivation, or via paracrine signalling driven by persistent SASP activity[24,25]. Although oncogene-induced senescence has been investigated in LGG, the effects of current standard of care therapies in inducing senescence has not been thoroughly investigated[19,26,27].

We sought to investigate the role of TIS in contributing to tumour regrowth after treatment withdrawal using the well-validated BT-40 PXA tumour cells. Our data supports the notion that current treatments against paediatric BRAF-V600E-activated glioma tumour can induce senescence. We identify that a combination therapy of Trametinib plus Navitoclax is effective in reducing rebound growth after treatment withdrawal.

Materials and Methods

Cells and reagents

BT-40 cells[13] (kind gift of Dr. P. Houghton, University of Texas) carrying BRAF-V600E together with CDKN2A/B loss, were maintained in RPMI1640 GlutaMAX (Gibco) with 10% FBS (Gibco). BT-40-LucF cells expressing Luciferase and GFP were generated via lentiviral transduction using pSLIEW vector with the previously described protocol[28]. H9-derived (WA09) human neural stem cells (hNSCs; Gibco - N7800) and H9 BRAF-V600E cells were grown on GelTrex (Thermo Fisher) in tumour stem media as previously described[29]. Extended protocols are in **Supplementary Material.**

DMSO (Santa Cruz Biotechnology [SCB]) was used as vehicle control; Dabrafenib (MedChemExpress [MCE] - HY-14660), Trametinib (ApexBio - A3018), Vinblastine (SCB - sc-491749), Navitoclax (ABT-262; ApexBio - A3007), A-1155463 (MCE - HY-19725), A-1331852 (MCE - HY-19741), Obatoclax (MCE - HY-10969), Venetoclax (ABT-199; ApexBio - A8194), Piperlongumine (ApexBio - A4455), Digoxin (ApexBio - B7684). BH3 mimetic characteristics are in **Table S1**.

ACCEPTED MANUSCRIPT

Downloaded from academic.oup.com/neuro-oncology/advance-article/doi/10.1093/neuonc/noag270/9004423 by Imperial College of Science Technology and Medicine user on 02 November 2026

Intracranial xenograft mouse model

Six-week-old female NOD scid gamma mice (Charles River UK) received right striatal stereotactic injections of 6×10^5 BT-40-LucF cells. Tumour growth was monitored every four days from day 12 via bioluminescence imaging (Firefly D-Luciferin, s.c 150mg/kg – PerkinElmer IVIS Lumina III). Mice were sacrificed upon >15% weight loss or neurological symptoms, followed by brightfield/GFP whole-mount brain imaging. Extended protocol in **Supplementary Material.**

FFPE immunofluorescence

Immunostaining on 4µm formalin-fixed paraffin-embedded sections were performed as described[30]. At least three tumours and between five to six non-consecutive slides were analysed. Imaging was performed on Zeiss Observer-7 (Hamamatsu Flash 4.0v3 camera, ZenBlue software v3.7). Quantification was performed with quPath software 0.5.1[31]. Antibodies and antigen retrieval methods are in **Table S2.**

Cell viability, drugs combinatorial effects and apoptosis

BT-40 were treated with indicated drugs for 72 h. Viability was measured via CellTiter-Glo assay (Promega) on a FLUOstar OPTIMA plate reader (BMG Labtech). IC50 and Drug Sensitivity Scores (DSS) were calculated using GraphPad Prism (v9.4.0) and Breeze-pipeline[32], respectively. Apoptosis was evaluated via Caspase-Glo 3/7 Assay (Promega), normalized to DAPI-positive nuclei. Extended protocol in **Supplementary Material**.

Bulk RNA-sequencing analysis

RNA was extracted using RNeasy Mini kit (Qiagen) as previously described[33], prepared with KAPA mRNA HyperPrep, and sequenced on an Illumina NextSeq2000. Data was aligned with STAR (v2.7.11b). Differential expression (DESeq2 v1.38.1) and GSEA were performed in R (v4.3.3). Genesets used were obtained from public databases: gene ontology, KEGG, REACTOME, molecular signatures database (Broad Institute); or published literature (senescence profiling and SASP[34,35]). Extended pipeline in **Supplementary Material.**

In vitro histochemistry and immunofluorescence

Proliferation and senescence were evaluated using Click-iT EdU (Invitrogen) and Senescence Cells Histochemical Staining (CS0030 - Sigma-Aldrich) kits, respectively. Fixed and permeabilized cells were immunostained and imaged on a Zeiss Observer7, with analysis in Fiji[36] (v1.53t). Protocols and antibody lists are supplemented in **Table S2**.

ACCEPTED MANUSCRIPT

Downloaded from academic.oup.com/neuro-oncology/advance-article/doi/10.1093/neuonc/noag270/9004423 by Imperial College of Science Technology and Medicine user on 02 November 2026

Statistical Analysis

Experiments were performed in biological triplicate. Data (mean ± SD for in vitro ; ± SEM for in vivo experiments) were analysed using GraphPad Prism v9.4.0 via appropriate tests and post-hoc tests indicated in figure legends. Kaplan-Meier survival was computed using the ggsurvfit v1.1.0 package. Significance was set at $p < 0.05$.

Results

Trametinib induces cell senescence and activates a myeloid attractant SASP in BT-40 tumour-bearing mice

First, we tested in vivo MAPK pathway inhibition using the MEK inhibitor Trametinib, which has been used alone or in combination with dabrafenib in pLGG clinical trials (NCT02124772). LucF-GFP BT-40 cells were orthotopically engrafted into NOD scid gamma (NSG) mice and tumour development was assessed by bioluminescence imaging (BLI). Once established (BLI> 3.10^6 $p.sec^{-1}.cm^{-2}.sr^{-1}$), mice were divided into two groups of equivalent BLI and treated with Trametinib (1mg/kg) or vehicle by oral gavage for 7 days (**Figure 1A**). As expected, Trametinib significantly reduced BLI compared with both the vehicle-treated group at the end of treatment (Day 14; p=0.0009) and with the BLI at treatment initiation (Day 0; p=0.0319). However, one week post-withdrawal, BLI levels in the Trametinib group increased again, indicating tumour regrowth (**Figure 1B**).

Next, we analysed BT-40 tumours by immunostaining for phosphorylated ERK1/2 (p-ERK1/2) to assess MAPK activation, Ki67 for proliferation, and HNA (human nuclear antigen) to identify BT-40 cells in mice treated with Trametinib for 7 days or examined 7 days after treatment withdrawal. Double immunofluorescence for p-ERK1/2 or Ki67 with HNA revealed a significant reduction in p-ERK1/2-positive and proliferating BT-40 cells in Trametinib-treated mice compared to vehicle controls (**Figure 1C-D)**. As expected, following Trametinib withdrawal, the proportion of BT-40 cells expressing p-ERK1/2 and Ki67 increased markedly relative to the Trametinib-treated tumours, reaching statistical significance for Ki67 (**Figure 1C-D**).

To explore whether Trametinib treatment leads to senescence induction, we analysed the expression of: (i) the cell cycle inhibitor *CDKN1A* ($p21^{Cip1}$), a key senescence mediator (*CDKN2A*, encoding $p16^{INK4a}$, another cell cycle regulator is deleted in BT-40 cells); (ii) the lysosomal enzyme β-galactosidase (encoded by *GLB1*), responsible for the senescence-associated β-galactosidase (SA-β-gal) staining; and (iii) the lysosomal membrane protein LAMP1. The expression of these markers was negligible in vehicle-treated controls but significantly elevated in

ACCEPTED MANUSCRIPT

Downloaded from academic.oup.com/neuro-oncology/advance-article/doi/10.1093/neuonc/noag270/9004423 by Imperial College of Science Technology and Medicine user on 02 November 2026

Trametinib-treated tumours (**Figure 1C-E**). After drug withdrawal, senescent marker expression was noticeably reduced, consistent with the increased Ki67 staining. These analyses suggest that Trametinib treatment results in MAPK pathway inhibition, decreased proliferation and concomitant expression of senescent markers in BT-40 cells, however, these responses are transient and diminish upon Trametinib withdrawal.

To validate this senescent phenotype molecularly, day 7 Trametinib-treated and vehicle-treated BT-40 tumours were dissociated, and tumour cells were FACS-isolated for bulk RNA-sequencing. Although low GFP expression limited FACS efficiency, with inefficient separation of BT-40 from murine brain cells, computational analysis of human transcripts allowed us to assess sample transcriptional variation. The data indicated substantial heterogeneity across BT-40 tumours, reflected by PCA plot dispersion (**Figure S1A**), with discernible separation between vehicle- and trametinib-treated groups. Differential expression analysis reaffirmed previously reported trametinib-induced changes, including upregulation of *CDKN1A* and SASP-related genes and repression of proliferation-associated genes (**Figure S1B; Table S3**). Geneset enrichment analysis (GSEA) revealed an enrichment for two active MAPK pathway associated gene sets in vehicle control group highlighting an inhibitory effect of trametinib on the MAPK pathway in BT-40 treated tumours (**Figure S1C**). Similarly, two proliferation-associated gene sets (e.g. E2F targets and cell cycle) were found to be enriched in vehicle control tumours (**Figure S1D**). Of note, the SenMAYO geneset[35], which contains a curated list of genes that characterises cellular senescence, as well as the SASP geneset[34], were enriched in Trametinib-treated BT-40 tumours, supporting the hypothesis that MAPK pathway inhibition by Trametinib results in senescence induction in BT-40 cells in vivo (**Figure S1E**).

Because the SASP can strongly influence immune cell recruitment, we examined SASP components in Trametinib-treated cells. Transcripts encoding chemokines CCL2, CXCL10, and the cytokine IL6 were markedly upregulated in senescent BT-40 cells (**Figure S1F**). Consistent with these transcriptomic data, double immunofluorescence with HNA showed a significant rise in the number of BT-40 tumour cells expressing each of these SASP factors in Trametinib-treated mice compared with vehicle controls (**Figure 2A-B**). Following Trametinib withdrawal, expression levels trended downward but did not reach statistical significance.

Given that CCL2, CXCL10, and IL6 play key roles in attracting and activating myeloid lineage cells[19], we next assessed myeloid infiltration. Immunofluorescence for IBA1 revealed abundant staining in Trametinib-treated tumours, whereas vehicle-treated tumours contained negligible IBA1-positive cells (**Figure 2A**). Notably, IBA1-

ACCEPTED MANUSCRIPT

Downloaded from academic.oup.com/neuro-oncology/advance-article/doi/10.1093/neuonc/noag270/9004423 by Imperial College of Science Technology and Medicine user on 02 November 2026

positive cells abundance increased even further after Trametinib withdrawal, despite the accompanying reduction in SASP factor expression (**Figure 2A,C**).

Overall, Trametinib suppresses proliferation and induces a senescence-associated program while activating a SASP that expands the IBA1-positive myeloid compartment in BT-40 tumour-bearing mice.

MAPKi and Vinblastine are capable of inducing cellular senescence and activating the SASP in BT-40 cells in vitro

We compared in vitro BT-40 responses to common paediatric glioma treatments: Trametinib, Dabrafenib, and Vinblastine. First, we carried out viability and apoptosis assays to identify the optimal conditions inducing cell cycle arrest with minimal effects on cell viability and apoptosis. BT-40 cells were cultured at increasing drug concentrations ranging from 10^{-10} to 10^{-6} M, and apoptosis and cell viability determined at day 1 and 3 post-drug treatment, respectively (**Figure S2A**). These studies revealed that drug concentrations up to 10^{-7} M (100 nM) caused minimal cell death or loss of cell viability (**Figure S2B**).

We next examined how these drugs influence BT-40 cell proliferation using two complementary experimental designs. In an extended-treatment paradigm, cells were continuously exposed to Dabrafenib, Trametinib, or Vinblastine at 1 nM, 5 nM, or 10 nM for 7 days before drug withdrawal. In a second, short-term exposure paradigm, cells were treated with 100 nM of each drug for 16 hours, after which the drug was removed, and cultures were maintained in drug-free media (**Figure S2C**). We reasoned that these two paradigms model distinct stages of treatment, initial response during exposure and behaviour after withdrawal. In both settings, EdU incorporation was measured on day 7 as a readout of proliferation, and cell confluence was monitored until day 35. Across both designs, all three drugs reduced EdU incorporation at 10 nM and 100 nM, consistent with cell-cycle arrest, whereas only Trametinib and Vinblastine reduced proliferation at 5 nM (**Figure S2D**). After drug withdrawal, the durability of the arrest differed markedly by drug and concentration. Removal of Dabrafenib or Trametinib allowed BT-40 cells to resume proliferation within two weeks at all concentrations tested (5 nM, 10 nM, and 100 nM). By contrast, withdrawal of Vinblastine induced a much more stable arrest that persisted through day 35, when the experiment concluded (**Figure S2E**).

Given that combined therapies are clinically relevant in paediatric glioma, we next evaluated the effects of Dabrafenib + Trametinib and Trametinib + Vinblastine, two regimens currently being evaluated in clinical trials

ACCEPTED MANUSCRIPT

Downloaded from academic.oup.com/neuro-oncology/advance-article/doi/10.1093/neuonc/noag270/9004423 by Imperial College of Science Technology and Medicine user on 02 November 2026

(NCT07110246, NCT04576117). At day 7 post-treatment, both combinations effectively inhibited cell proliferation and triggered a robust increase in SA-β-Gal activity compared with vehicle-treated controls, although these effects were not greater than those observed with the respective single agents (**Figure S3A-C**). Furthermore, given recent therapeutic developments, we assessed the effect of the type II RAF inhibitor Tovorafenib. Treatment with 100 nM Tovorafenib for 24 hours produced a comparable reduction in cell proliferation and increase in SA-β-Gal activity at day 7, similar to the effects observed with Dabrafenib (**Figure S3D-F**). Together, these results indicate that both combination therapies and type II RAF inhibition induce features of senescence in BT-40 cells.

We next characterized this senescent phenotype molecularly. Based on the previously described findings, we utilized the 16-hour treatment and wash-out paradigm, as this brief exposure produced a durable, homogeneous growth arrest consistent with a stable senescence-like state. At day 7, staining revealed a significant increase of both SA-β-gal and $p21^{CIP1}$-expressing cells suggesting senescence induction (**Figure 3B-C**). To confirm this phenotype, we performed bulk RNA sequencing of BT-40 cells 7 days after short-term treatment with Dabrafenib, Trametinib or Vinblastine and vehicle control. As expected, the transcriptomic profiles of the treated cells were highly altered compared to vehicle controls, evidenced by volcano plots (**Figure 3D**), experimental group separation in PCA plots (**Figure S4A**), and unsupervised ranking of the top 500 differentially expressed genes (**Figure S4B**). Gene pathway analysis revealed the enrichment of pathways associated with cell proliferation in the vehicle treated BT-40 cells (**Figure 3E**). In contrast, treatment with either of the drugs resulted in the significant enrichment of pathways related to senescence, SASP and SASP-associated biological processes. Supporting the RNAseq data, immunofluorescence staining confirms the expression of IL1β in Dabrafenib and Vinblastine-treated cells, as well as CCL2 in Dabrafenib, Trametinib, and to a lesser extend Vinblastine-treated cells (**Figure 3F**). These observations are consistent with selected SASP component expression represented in heatmap (**Figure 3G**).

Although the three treatments were able to induce senescence and SASP, we noticed that there were differences in the dysregulated genes among treatments, suggesting drug-specific responses (**Figures 3D, S4C**). When comparing the transcriptomes of the differentially expressed genes (DEGs) between treated cells and controls, we identified a core signature comprising 132 genes shared between the three treatments, which included senescence and SASP genes such as *CDKN1A* (encoding the cell cycle inhibitor $p21^{CIP1}$ - **Figure S4D**),

ACCEPTED MANUSCRIPT

Downloaded from academic.oup.com/neuro-oncology/advance-article/doi/10.1093/neuonc/noag270/9004423 by Imperial College of Science Technology and Medicine user on 02 November 2026

SUSD2 (involved in negative regulation of cell cycle), and secreted factors such as *IL6*, *CXCL10*, *CCL2*, *PDGFB* and *VEGFA*. These RNA-seq data are consistent with and further support our in vivo immunofluorescence findings (**Figures 1C-E, 2A-B**), showing consistent upregulation at both the transcript and protein levels of key senescence and SASP markers, notably p21, IL6, CXCL10, and CCL2. Trametinib-treatment induced drastic transcriptomic changes with 1363 specific DEGs, which included many lysosome-associated genes, suggesting lysosomal expansion, a hallmark of senescence (**Figure S4C,E**). Additionally, *CXCL6*, *CSF1*, *TIMP2* and matrix components *COL1A1*, *COL3A1* and *COL5A2* were specifically upregulated in Trametinib-treated cells (**Figure 3G, Tables S4-S5-S6).** Other SASP components, e.g. *IL1A*, *IL1B*, *TGFB1* and metalloproteases *MMP8* and *MMP17* were upregulated in Dabrafenib and Vinblastine-treated cells, but not in Trametinib-induced senescence state. Together, these analyses demonstrate that while BT-40 cells treated with Trametinib, Dabrafenib, or Vinblastine display senescent signatures in vitro, the extent and pattern of SASP gene upregulation differ depending on the specific drug used.

To assess generalizability in BRAF-V600E-altered pLGG models, we examined H9-derived human neural stem cells (hNSCs) stably expressing *BRAF-V600E* (H9 BRAF-V600E), which we previously showed confers growth factor independence and immortalization[29]. Viability and apoptosis assays confirmed these cells exhibit increased sensitivity to MAPK inhibition by Dabrafenib and Trametinib compared to H9 WT cells under conditions analogous to BT-40 experiments (**Figure S5A**). Consistent with a dependence on MAPK signalling, H9 BRAF-V600E cells were more sensitive to both Dabrafenib (IC50: 0.012 µM vs. 0.13 µM in WT) and Trametinib (IC50: 4.17×10^{-5} µM vs. 1.12 µM in WT), whereas both cell lines exhibited comparable sensitivity to Vinblastine (**Figure S5B-C**).

We then evaluated senescence induction in H9 BRAF-V600E cells using either a one-day high-dose treatment followed by recovery, or a six-day lower-dose continuous paradigm, analogous to the BT-40 experiments (**Figure S6A**). Relative to DMSO-treated controls, both treatment regimens with Dabrafenib, Trametinib or Vinblastine significantly increased SA-β-gal positivity (**Figure S6B**). Furthermore, short-term and continuous exposures significantly reduced cell growth ($p < 0.01$) and EdU incorporation ($p < 0.001$) (**Figure S6C-D**). Together, these findings demonstrate that, similar to the BT-40 patient-derived glioma model, BRAF-V600E-expressing H9 hNSCs undergo growth arrest and acquire hallmarks of cellular senescence following targeted BRAF-V600E inhibition, MAPK pathway blockade, or cytotoxic chemotherapy.

ACCEPTED MANUSCRIPT

Downloaded from academic.oup.com/neuro-oncology/advance-article/doi/10.1093/neuonc/noag270/9004423 by Imperial College of Science Technology and Medicine user on 02 November 2026

Senescent BT-40 tumour cells are highly sensitive to Bcl-xL inhibition

We explored whether therapy-induced senescence in BT-40 cells could be therapeutically exploited using senolytics. We tested three described senolytic agents, Piperlongumine, Digoxin, and Navitoclax on senescence-induced (i.e. previously treated with Dabrafenib, Trametinib or Vinblastine) and control proliferative, vehicle-treated BT-40 cells (**Figure 4A)**. Only Navitoclax selectively ablated senescent cells in a dose response manner (**Figures 4B-C, S7**). Compared to proliferative cells, senescent cells induced by Dabrafenib, Trametinib, or Vinblastine were 6-, 50-, and 7-fold more sensitive to Navitoclax, respectively (**Figure 4C**). Notably, BT-40 cells treated with combinations (Dabrafenib + Trametinib or Trametinib + Vinblastine) or Tovorafenib also displayed high Navitoclax sensitivity (IC50 values: 20 nM, 37 nM, 20 nM, respectively) (**Figure S3G**). Confirming these differences in responses to Navitoclax treatment, ssGSEA (single-sample GSEA) was used to calculate enrichment scores for each individual sample[26,37]. ssGSEA revealed that treatment with either of the drugs resulted in higher Navitoclax-sensitivity and a lower Navitoclax-resistance relative to proliferative control BT40 cells **(Figure 4D**). Of note, the highest Navitoclax-sensitivity and lowest Navitoclax-resistance scores were observed in Trametinib-induced senescent BT-40 cells.

Navitoclax can inhibit Bcl-2, Bcl-xL, and Bcl-w [38]. To identify the specific protein underlying the senolytic effect of Navitoclax, we tested BH3 mimetics with specific inhibitory profiles. Drug sensitivity scores (DSS) from dose-response curves were mapped (**Figure 4B**). Venetoclax, a weak Bcl-xL inhibitor, yielded DSS <15 across treatments. In contrast, DSS values obtained for inhibitors with strong affinity to Bcl-xL such as Navitoclax, the pan-Bcl2 inhibitor Obatoclax or, more relevant, the selective Bcl-xL inhibitors A-1155463 and A-1331852, were greater than 25, suggesting a higher sensitivity of treatment-induced senescent BT-40 cells to Bcl-xL inhibition (**Figures 4B, S7A-F**). To further confirm that BT-40 cells upregulate Bcl-xL under therapy-induced senescence conditions, we evaluated its protein expression by immunofluorescence. Consistent with our pharmacological findings, we demonstrated that following Trametinib treatment, BT-40 cells significantly upregulate the Bcl-xL protein (**Figure S7G**). Comparing Navitoclax IC50 values to the GDSC database (Genomics of Drug Sensitivity in Cancer - 928 cell lines) revealed that therapy-induced senescent BT-40 cells rank among the most sensitive lines, with trametinib-induced senescence 2nd, dabrafenib-induced senescence 17th, and vinblastine-induced senescence 50th (**Figure S7H**).

ACCEPTED MANUSCRIPT

Downloaded from academic.oup.com/neuro-oncology/advance-article/doi/10.1093/neuonc/noag270/9004423 by Imperial College of Science Technology and Medicine user on 02 November 2026

Finally, inhibition of BCL-xL is expected to result in apoptosis. Navitoclax treatment (0.1µM and 1.0mM) increased effector caspase 3/7 activity in senescent cells, suggesting induction of apoptosis (**Figure 4E**). Together, these studies point toward a selective vulnerability of treatment-induced senescent BT-40 tumour cells to apoptosis upon Bcl-xL inhibition, with Trametinib-treated cells showing the greatest sensitivity to Navitoclax.

Combined Trametinib and Navitoclax therapy reduces tumour burden and prolongs survival in BT-40 tumour-bearing mice

We next evaluated the efficacy of combined Trametinib and Navitoclax therapy in NSG mice orthotopically transplanted with BT-40-LucF cells. Once BLI reached 3.10^6 $p.sec^{-1}.cm^{-2}.sr^{-1}$, mice were evenly distributed into four groups with comparable tumour burdens: (1) Vehicle control, receiving the oral vehicle used for Trametinib and Navitoclax (n = 5); (2) Navitoclax, 50 mg/kg/day via oral gavage, 5 days per week for 2 weeks (n = 5); (3) Trametinib, 1 mg/kg/day via oral gavage, 5 days per week for 3 weeks (n = 7); (4) Combination therapy (Trametinib for 1 week, followed by Trametinib plus Navitoclax for 2 weeks at identical doses/schedules; n=9) (**Figure 5A**). Treatments were well-tolerated. While Navitoclax monotherapy did not affect body weight, combination therapy caused a mild, transient weight reduction (<5% loss) without clinical signs of distress or toxicity (**Figure S8A**).

Median survival was 54 days for vehicle controls, 55 days for Navitoclax, and 78 days for Trametinib (**Figure 5B**). Remarkably, in the combination group, 4/9 mice survive until day 150 without neurological symptoms, with log-rank tests confirming significant survival differences. Average BLI fold-change showed significant reductions in the Trametinib and combination groups (**Figure 5C**). Examining individual mice, the combination group displayed variable responses: 5/9 showed increased BLI post-withdrawal, while 4/9 exhibited remarkable progressive BLI decreases to nearly undetectable levels (**Figures 5D, S8B**). These findings demonstrate significant anti-tumour activity of the Trametinib and Navitoclax combination against BT-40 tumours, albeit with intra-group heterogeneity in the duration of treatment efficacy.

Investigating underlying mechanisms, tumours were analysed during treatment via double immunofluorescence with an anti-HNA antibody. Both Trametinib-only and combination treatments significantly reduced the proliferative index compared to vehicle and Navitoclax-only groups (**Figure 5E-F**). Conversely, apoptosis

ACCEPTED MANUSCRIPT

Downloaded from academic.oup.com/neuro-oncology/advance-article/doi/10.1093/neuonc/noag270/9004423 by Imperial College of Science Technology and Medicine user on 02 November 2026

(indicated by cleaved caspase-3) was significantly increased only in the combination group relative to all other cohorts (**Figure 5E**). Senescent markers ($p21^{CIP1}$, GLB1, LAMP1) were elevated in the Trametinib-only group compared to controls, as previously shown (**Figures 1C-E, 5E-F, S9A-B**). Crucially, senescent marker expression in the combination group was significantly reduced compared to the Trametinib-only group (**Figures 5E-F, S9A-B**).

Finally, analysing the myeloid compartment via IBA1 and HNA double immunostaining confirmed abundant IBA1-expressing myeloid cells in Trametinib-only tumours (**Figure 6A-B**). Remarkably, IBA1-positive cells numbers were vastly reduced in the combination group compared to Trametinib alone (**Figure 6C**). This reduction correlated with significantly decreased CCL2-, CXCL10-, and IL6-expressing cells (**Figure S9C-D**). Together, these analyses confirm Trametinib induces senescence in BT-40 cells, while Navitoclax ablates these senescent cells, thereby decreasing chemokine expression and reducing myeloid tumour infiltration.

Discussion

In this study, we demonstrate that therapies used or being evaluated for paediatric BRAF-V600E-mutant gliomas, including the MEK inhibitor Trametinib, the BRAF-V600E inhibitor Dabrafenib, the type II RAF inhibitor Tovorafenib and the chemotherapeutic agent Vinblastine, induce features of cellular senescence in BT-40 tumour cells in vitro, either as single agents or in combination. Furthermore, we demonstrate that Trametinib treatment induces a senescence phenotype in vivo and that combining Trametinib with the senolytic agent Navitoclax significantly enhances therapeutic efficacy. We show that this senescent state is associated with the activation of a SASP, leading to increased secretion of pro-inflammatory cytokines and recruitment of $IBA1^{+}$ myeloid cells within the tumour microenvironment. Notably, despite *CDKN2A/B* deletion in BT-40 cells, which prevents $p16^{INK4a}$-dependent senescence[13], these tumour cells are able to activate a treatment-induced senescence program, most likely through CDKN1A ($p21^{Cip1}$) expression, suggesting that MAPK pathway inhibition triggers a p53/p21-driven arrest in this model. We identify Navitoclax as a potent senolytic agent capable of eliminating therapy-induce senescent BT-40 cells and reducing or even preventing tumour rebound growth upon Trametinib withdrawal. Combination therapy with Trametinib and Navitoclax significantly reduces tumour

ACCEPTED MANUSCRIPT

Downloaded from academic.oup.com/neuro-oncology/advance-article/doi/10.1093/neuonc/noag270/9004423 by Imperial College of Science Technology and Medicine user on 02 November 2026

burden and prolongs survival in a preclinical BT-40 orthotopic mouse model, highlighting a promising therapeutic strategy for paediatric gliomas carrying BRAF-V600E mutations.

Although all three drugs induced therapy-induced senescence (TIS), our transcriptomic analyses revealed drug-specific SASP profiles. Trametinib treatment induced stronger upregulation of lysosomal genes, extracellular matrix components (COL1A1, COL3A1, COL5A2), and cytokines such as CXCL6, CSF1, and TIMP2, whereas Dabrafenib and Vinblastine preferentially upregulated IL1A, IL1B, TGFB1, and MMP17. These observations are consistent with emerging evidence that TIS does not represent a uniform biological program but instead produces highly context-dependent SASP signatures, strongly influenced by the nature of the inducing agent[39]. For example, CDK4/6 inhibition can drive a SASP enriched in immune-stimulatory chemokines such as CXCL9, CXCL10, and MICB, enhancing NK and T cell recruitment[40], whereas genotoxic agents like docetaxel induce a pro-metastatic and immunosuppressive SASP[41,42]. In our model, the distinct SASP profiles triggered by Trametinib, Dabrafenib, and Vinblastine likely contribute to differential immune modulation within the tumour microenvironment and may explain variability in therapeutic efficacy. Beyond TIS, the SASP is increasingly recognised as an intrinsic feature of pLGG biology driven by oncogene-induced senescence (OIS). Recent studies have shown that SASP signalling is already active in pLGG and may contribute to both tumour maintenance and microenvironmental crosstalk[27]. This raises the possibility that MAPK inhibitor-induced senescence occurs within a cellular context already conditioned by OIS-associated SASP activity. In such a landscape, pharmacologically-induced senescence may not only reinforce pre-existing SASP programmes but also amplify inflammatory and immune-modulatory signalling, potentially enhancing the myeloid responses and tumour–stroma interactions we observe.

A striking finding of our study is that Trametinib-induced senescence was accompanied by the secretion of microglia-attracting chemokines and cytokines, including CCL2, CXCL10, and IL6, which correlated with an expansion of IBA1+ myeloid cells within the tumour microenvironment. Although microglia have context-dependent roles in glioma progression, recent studies suggest that their recruitment by senescent cells may promote an immunosuppressive environment and facilitate tumour regrowth after treatment withdrawal[19,43,44]. Our data showing persistent IBA1+ myeloid cells infiltration even after Trametinib discontinuation, despite partial reduction of SASP cytokines, suggest that therapy-induced changes in the tumour microenvironment may predispose to tumour rebound. These findings are consistent with reports in paediatric low-grade gliomas

ACCEPTED MANUSCRIPT

Downloaded from academic.oup.com/neuro-oncology/advance-article/doi/10.1093/neuonc/noag270/9004423 by Imperial College of Science Technology and Medicine user on 02 November 2026

demonstrating that MAPK pathway inhibition leads to compensatory immune responses, which may undermine long-term therapeutic efficacy[45,46].

We identify Navitoclax, a well-characterised senolytic targeting BCL-2 family proteins, as a potent inducer of apoptosis in TIS BT-40 cells. Using selective inhibitors against individual anti-apoptotic proteins, we reveal that blockade of BCL-xL is the principal mechanism underlying Navitoclax's activity. This aligns with previous reports showing that senescent cells depend on anti-apoptotic signalling for survival and are therefore preferentially susceptible to BCL-xL inhibition[47]. Notably, treatment-induced senescent BT-40 cells displayed markedly lower IC50 values for Navitoclax than proliferative BT-40 cells, with Trametinib-induced senescent cells showing the greatest sensitivity. These findings parallel those of Sigaud et al., who reported strong synergy between the ERK inhibitor ulixertinib and BH3-mimetics, particularly the BCL-xL inhibitor Navitoclax, across multiple BRAF-driven pLGG models[48]. Moreover, BCL-xL inhibition has previously been proposed as a therapeutic vulnerability in pLGG in the setting of OIS[26]. Our results extend this vulnerability to TIS, suggesting that combining BCL-xL inhibition with MAPK pathway blockade may offer a dual strategy to eliminate both OIS- and TIS-associated senescent cell populations within the tumour.

In vivo, a combination therapy with Trametinib and Navitoclax leads to significant tumour regression, prolonged survival, reduced SASP cytokine expression, and decreased myeloid infiltration, providing proof-of-concept for a senolytic-based therapeutic approach in paediatric gliomas. Our data also suggest that the benefits of Navitoclax are not merely due to tumour debulking but rather to the selective removal of senescent cells, thereby reducing pro-tumorigenic SASP-driven microenvironmental changes.

Our findings support a novel therapeutic paradigm in paediatric BRAF-V600E gliomas: combining MAPK pathway inhibitors with senolytics to enhance treatment efficacy and reduce tumour regrowth after drug withdrawal. This strategy may have relevance in preventing long-term dependence on targeted therapies, which can be associated with cumulative toxicity, quality-of-life impairment, and risk of malignant progression[49]. However, translating our results into the clinic requires addressing several key challenges including toxicity concerns. Navitoclax is indeed associated with dose-limiting thrombocytopenia in paediatric and adult trials[50], developing BCL-xL-selective inhibitors or intermittent dosing schedules may improve tolerability[47]. Another aspect is patient heterogeneity, given the context-dependent nature of SASP profiles, identifying predictive biomarkers of both senescence induction and senolytic susceptibility will be essential to design therapeutic strategies. Moreover,

ACCEPTED MANUSCRIPT

Downloaded from academic.oup.com/neuro-oncology/advance-article/doi/10.1093/neuonc/noag270/9004423 by Imperial College of Science Technology and Medicine user on 02 November 2026

blood-brain barrier (BBB) penetration of Navitoclax may be limited, although recent evidence in primates has demonstrated that this compounds can cross the BBB and accumulate in the cerebrospinal fluid at concentrations able to ablate senescent cells [51]. Finally, this emerging 'one-two punch' therapeutic paradigm is likely to depend on optimal treatment sequencing, and the therapeutic window for senolytic administration relative to MAPK inhibition remains an important open question. This is particularly relevant given findings from a recent phase I/II trial evaluating Navitoclax in combination with Trametinib in patients with KRAS/NRAS-mutant advanced solid tumours[52]. Despite strong preclinical rationale, the combination achieved a relatively low response rate (16%). These findings highlight the challenges of translating senolytic strategies into clinical benefit and emphasise the importance of defining optimal treatment schedules, identifying robust biomarkers and selecting appropriate patient populations. Future studies should evaluate this combination strategy across diverse BRAF-mutant glioma models, integrate immune profiling to better understand microglial dynamics, and explore senolytic alternatives with improved safety profiles.

While our findings provide strong preclinical evidence, several limitations should be considered, including that our analyses are based primarily on the BT-40 cell line, one of the few well-characterised, patient-derived models available for BRAF-V600E-mutant paediatric gliomas. BT-40 was derived from a pleomorphic xanthoastrocytoma (PXA) harbouring a *CDKN2A/B* deletion. PXA can exhibit a more aggressive, high-grade clinical course than typical pLGG, with a correspondingly different long-term clinical trajectory. Nevertheless, PXA tumours can display a pronounced rebound phenomenon following MAPK inhibitor withdrawal, making BT-40 a useful model for investigating the biological mechanisms underlying tumour regrowth, while recognising that it does not fully recapitulate the indolent biology of classical pLGG. Broader validation in additional paediatric glioma models is warranted. Although we demonstrate SASP-driven myeloid recruitment, the functional role of these cells, whether pro-tumorigenic or anti-tumorigenic, remains to be elucidated.

Our study uncovers a previously unappreciated role of therapy-induced senescence in shaping the response of paediatric BRAF-V600E gliomas to current standard treatments. We demonstrate that senescent BT-40 tumour cells exhibit a selective vulnerability to BCL-xL inhibition, and that combining Trametinib with Navitoclax effectively reduces tumour burden, suppresses SASP-driven microenvironmental changes, and reduce or prevent tumour regrowth after Trametinib withdrawal. These findings provide a strong preclinical rationale for integrating senolytics into therapeutic regimens for paediatric gliomas carrying BRAF-V600E mutations.

ACCEPTED MANUSCRIPT

Downloaded from academic.oup.com/neuro-oncology/advance-article/doi/10.1093/neuonc/noag270/9004423 by Imperial College of Science Technology and Medicine user on 02 November 2026

Required statements

Ethics. All mouse procedures were performed under licence, following UK Home Office Animals (Scientific Procedures) Act 1986, ARRIVE guidelines, and local institutional guidelines (UCL ethical review committee). A humane endpoint was chosen to avoid severe adverse effects and minimise suffering of mice harbouring tumours, according to UK Home Office and local Ethical Committee regulations.

Funding. Cancer Research UK (C54322/A27727 to J.P.M-B.; C15075/A28647, DRCPGM-Jun25/100003 to J.G.); The Brain Tumour Charity and The Everest Centre for Low-grade Paediatric Brain Tumours (GN-000707 to J.P.M-B. and T.M.); National Institute for Health and Care Research Biomedical Research Centre at Great Ormond Street Hospital for Children NHS Foundation Trust and University College London (to J.P.M-B.); Medical Research Council (MC_U120085810 to J.G.).

Conflict of Interest. J.G. has acted as a consultant for Unity Biotechnology, Geras Bio, Myricx Pharma, and Merck KGaA. Pfizer and Unity Biotechnology have funded research in J.G.'s lab (unrelated to the work presented here). J.G. owns equity in Geras Bio. J.G.is a named inventor in MRC and Imperial College patents, both related to senolytic therapies (the patents are not related to the work presented here). T.M. is advisory board member of Ipsen Pharma GmbH.

Authorship. RG and HH carried out most of the experiments and prepared all the figure panels for publication. AV, LC provided expertise and carried out brain cell injection. RS carried out the analysis shown in Figure 4D. THC and RK carried out human neural stem cells experiments. SB conducted Bcl-xL immunofluorescence experiments. GC, SH, AB, DG contributed experimentally. DH, JG, OW, TM, PB, PA, FS provided expertise and intellectual input. The project was designed by RG and JPMB. RG and JPMB wrote the paper, with help from HH. All authors reviewed and approved this submission.

Data availability. Raw and processed RNA sequencing data are available on GEO repository GSE294664 and GSE296000. Complete analysis pipeline is available at https://gitlab.univ-nantes.fr/guihomics/plgg_tis_rnaseq

Acknowledgements

ACCEPTED MANUSCRIPT

Downloaded from academic.oup.com/neuro-oncology/advance-article/doi/10.1093/neuonc/noag270/9004423 by Imperial College of Science Technology and Medicine user on 02 November 2026

We thank core facilities such as UCL Genomics, Light Microscopy facility and UCL Biological Services Unit. We thank Prof. Owen Williams (University College London) for providing LucF-GFP lentiviral vector. We thank our funders and sponsors for enabling the research presented in this manuscript.

ACCEPTED MANUSCRIPT

Downloaded from academic.oup.com/neuro-oncology/advance-article/doi/10.1093/neuonc/noag270/9004423 by Imperial College of Science Technology and Medicine user on 02 November 2026

References

1. Fangusaro J, Jones DT, Packer RJ, et al. Pediatric low-grade glioma: State-of-the-art and ongoing challenges. *Neuro Oncol*. 2023;26(1):25-37. doi:10.1093/neuonc/noad195

2. Schiff D, Brown PD, Giannini C. Outcome in adult low-grade glioma: the impact of prognostic factors and treatment. *Neurology*. 2007;69(13):1366-1373. doi:10.1212/01.wnl.0000277271.47601.a1

3. Ryall S, Tabori U, Hawkins C. Pediatric low-grade glioma in the era of molecular diagnostics. *acta neuropathol commun*. 2020;8(1):30. doi:10.1186/s40478-020-00902-z

4. Jones DTW, Hutter B, Jäger N, et al. Recurrent somatic alterations of FGFR1 and NTRK2 in pilocytic astrocytoma. *Nat Genet*. 2013;45(8):927-932. doi:10.1038/ng.2682

5. Jones DTW, Bandopadhayay P, Jabado N. The Power of Human Cancer Genetics as Revealed by Low-Grade Gliomas. *Annu Rev Genet*. 2019;53(1):483-503. doi:10.1146/annurev-genet-120417-031642

6. Jacob K, Quang-Khuong DA, Jones DTW, et al. Genetic Aberrations Leading to MAPK Pathway Activation Mediate Oncogene-Induced Senescence in Sporadic Pilocytic Astrocytomas. *Clinical Cancer Research*. 2011;17(14):4650-4660. doi:10.1158/1078-0432.CCR-11-0127

7. Zureick AH, Evans CL, Niemierko A, et al. Left hippocampal dosimetry correlates with visual and verbal memory outcomes in survivors of pediatric brain tumors. *Cancer*. 2018;124(10):2238-2245. doi:10.1002/cncr.31143

8. Schiffman JD, Hodgson JG, VandenBerg SR, et al. Oncogenic *BRAF* Mutation with *CDKN2A* Inactivation Is Characteristic of a Subset of Pediatric Malignant Astrocytomas. *Cancer Research*. 2010;70(2):512-519. doi:10.1158/0008-5472.CAN-09-1851

9. Reinhardt A, Stichel D, Schrimpf D, et al. Anaplastic astrocytoma with piloid features, a novel molecular class of IDH wildtype glioma with recurrent MAPK pathway, CDKN2A/B and ATRX alterations. *Acta Neuropathol*. 2018;136(2):273-291. doi:10.1007/s00401-018-1837-8

10. Pollack IF, Agnihotri S, Broniscer A. Childhood brain tumors: current management, biological insights, and future directions: JNSPG 75th Anniversary Invited Review Article. *Journal of Neurosurgery: Pediatrics*. 2019;23(3):261-273. doi:10.3171/2018.10.PEDS18377

11. Lassaletta A, Scheinemann K, Zelcer SM, et al. Phase II Weekly Vinblastine for Chemotherapy-Naïve Children With Progressive Low-Grade Glioma: A Canadian Pediatric Brain Tumor Consortium Study. *J Clin Oncol*. 2016;34(29):3537-3543. doi:10.1200/JCO.2016.68.1585

12. Kolb EA, Gorlick R, Houghton PJ, et al. Initial testing (stage 1) of AZD6244 (ARRY-142886) by the pediatric preclinical testing program. *Pediatric Blood & Cancer*. 2010;55(4):668-677. doi:10.1002/pbc.22576

13. Bid HK, Kibler A, Phelps DA, et al. Development, Characterization, and Reversal of Acquired Resistance to the MEK1 Inhibitor Selumetinib (AZD6244) in an In Vivo Model of Childhood Astrocytoma. *Clin Cancer Res*. 2013;19(24):6716-6729. doi:10.1158/1078-0432.CCR-13-0842

14. Fangusaro J, Onar-Thomas A, Young Poussaint T, et al. Selumetinib in paediatric patients with *BRAF*-aberrant or neurofibromatosis type 1-associated recurrent, refractory, or progressive low-grade glioma: a multicentre, phase 2 trial. *The Lancet Oncology*. 2019;20(7):1011-1022. doi:10.1016/S1470-2045(19)30277-3

15. Banerjee A, Jakacki RI, Onar-Thomas A, et al. A phase I trial of the MEK inhibitor selumetinib (AZD6244) in pediatric patients with recurrent or refractory low-grade glioma: a Pediatric Brain Tumor Consortium (PBTC) study. *Neuro-Oncology*. 2017;19(8):1135-1144. doi:10.1093/neuonc/now282

ACCEPTED MANUSCRIPT

Downloaded from academic.oup.com/neuro-oncology/advance-article/doi/10.1093/neuonc/noag270/9004423 by Imperial College of Science Technology and Medicine user on 02 November 2026

16. Bouffet E, Hansford JR, Garrè ML, et al. Dabrafenib plus Trametinib in Pediatric Glioma with BRAF V600 Mutations. *New England Journal of Medicine*. 2023;389(12):1108-1120. doi:10.1056/NEJMoa2303815

17. Bouffet E, Geoerger B, Moertel C, et al. Efficacy and Safety of Trametinib Monotherapy or in Combination With Dabrafenib in Pediatric BRAF V600–Mutant Low-Grade Glioma. *JCO*. 2023;41(3):664-674. doi:10.1200/JCO.22.01000

18. Nobre L, Zapotocky M, Ramaswamy V, et al. Outcomes of BRAF V600E Pediatric Gliomas Treated With Targeted BRAF Inhibition. *JCO Precis Oncol*. 2020;(4):561-571. doi:10.1200/PO.19.00298

19. Kocher D, Cao L, Guiho R, et al. Rebound growth of BRAF mutant pediatric glioma cells after MAPKi withdrawal is associated with MAPK reactivation and secretion of microglia-recruiting cytokines. *J Neurooncol*. 2024;168(2):317-332. doi:10.1007/s11060-024-04672-9

20. Gorgoulis V, Adams PD, Alimonti A, et al. Cellular Senescence: Defining a Path Forward. *Cell*. 2019;179(4):813-827. doi:10.1016/j.cell.2019.10.005

21. Wang L, Lankhorst L, Bernards R. Exploiting senescence for the treatment of cancer. *Nat Rev Cancer*. 2022;22(6):340-355. doi:10.1038/s41568-022-00450-9

22. He S, Sharpless NE. Senescence in Health and Disease. *Cell*. 2017;169(6):1000-1011. doi:10.1016/j.cell.2017.05.015

23. Demaria M, O'Leary MN, Chang J, et al. Cellular Senescence Promotes Adverse Effects of Chemotherapy and Cancer Relapse. *Cancer Discovery*. 2017;7(2):165-176. doi:10.1158/2159-8290.CD-16-0241

24. Paez-Ribes M, González-Gualda E, Doherty GJ, Muñoz-Espín D. Targeting senescent cells in translational medicine. *EMBO Molecular Medicine*. 2019;11(12):e10234. doi:10.15252/emmm.201810234

25. Gonzalez-Meljem JM, Apps JR, Fraser HC, Martinez-Barbera JP. Paracrine roles of cellular senescence in promoting tumourigenesis. *Br J Cancer*. 2018;118(10):1283-1288. doi:10.1038/s41416-018-0066-1

26. Selt F, Sigaud R, Valinciute G, et al. BH3 mimetics targeting BCL-XL impact the senescent compartment of pilocytic astrocytoma. *Neuro Oncol*. 2022;25(4):735-747. doi:10.1093/neuonc/noac199

27. Buhl JL, Selt F, Hielscher T, et al. The Senescence-associated Secretory Phenotype Mediates Oncogene-induced Senescence in Pediatric Pilocytic Astrocytoma. *Clinical Cancer Research*. 2019;25(6):1851-1866. doi:10.1158/1078-0432.CCR-18-1965

28. Brion R, Gantier M, Biteau K, et al. TRAIL-Based Therapies Efficacy in Pediatric Bone Tumors Models Is Modulated by TRAIL Non-Apoptotic Pathway Activation via RIPK1 Recruitment. *Cancers (Basel)*. 2022;14(22):5627. doi:10.3390/cancers14225627

29. Apfelbaum AA, Morin E, Sturm D, et al. A diverse landscape of FGFR alterations and co-mutations suggests potential therapeutic strategies in pediatric low-grade gliomas. *Nat Commun*. 2025;16(1):7018. doi:10.1038/s41467-025-61820-z

30. Carreno G, Boult JKR, Apps J, et al. SHH pathway inhibition is protumourigenic in adamantinomatous craniopharyngioma. *Endocrine-Related Cancer*. 2019;26(3):355-366. doi:10.1530/ERC-18-0538

31. Bankhead P, Loughrey MB, Fernández JA, et al. QuPath: Open source software for digital pathology image analysis. *Sci Rep*. 2017;7(1):16878. doi:10.1038/s41598-017-17204-5

32. Potdar S, Ianevski A, Mpindi JP, et al. Breeze: an integrated quality control and data analysis application for high-throughput drug screening. *Bioinformatics*. 2020;36(11):3602-3604. doi:10.1093/bioinformatics/btaa138

ACCEPTED MANUSCRIPT

Downloaded from academic.oup.com/neuro-oncology/advance-article/doi/10.1093/neuonc/noag270/9004423 by Imperial College of Science Technology and Medicine user on 02 November 2026

33. Haston S, Gonzalez-Gualda E, Morsli S, et al. Clearance of senescent macrophages ameliorates tumorigenesis in KRAS-driven lung cancer. *Cancer Cell*. 2023;41(7):1242-1260.e6. doi:10.1016/j.ccell.2023.05.004

34. Fridman AL, Tainsky MA. Critical pathways in cellular senescence and immortalization revealed by gene expression profiling. *Oncogene*. 2008;27(46):5975-5987. doi:10.1038/onc.2008.213

35. Saul D, Kosinsky RL, Atkinson EJ, et al. A new gene set identifies senescent cells and predicts senescence-associated pathways across tissues. *Nat Commun*. 2022;13(1):4827. doi:10.1038/s41467-022-32552-1

36. Schindelin J, Arganda-Carreras I, Frise E, et al. Fiji: an open-source platform for biological-image analysis. *Nat Methods*. 2012;9(7):7. doi:10.1038/nmeth.2019

37. Marczyk M, Patwardhan GA, Zhao J, et al. Multi-Omics Investigation of Innate Navitoclax Resistance in Triple-Negative Breast Cancer Cells. *Cancers*. 2020;12(9):9. doi:10.3390/cancers12092551

38. Tse C, Shoemaker AR, Adickes J, et al. ABT-263: a potent and orally bioavailable Bcl-2 family inhibitor. *Cancer Res*. 2008;68(9):3421-3428. doi:10.1158/0008-5472.CAN-07-5836

39. Colucci M, Sarill M, Maddalena M, et al. Senescence in cancer. *Cancer Cell*. 2025;43(7):1204-1226. doi:10.1016/j.ccell.2025.05.015

40. Lee DH, Imran M, Choi JH, et al. CDK4/6 inhibitors induce breast cancer senescence with enhanced anti-tumor immunogenic properties compared with DNA-damaging agents. *Molecular Oncology*. 2024;18(1):216-232. doi:10.1002/1878-0261.13541

41. Di Mitri D, Toso A, Chen JJ, et al. Tumour-infiltrating Gr-1+ myeloid cells antagonize senescence in cancer. *Nature*. 2014;515(7525):134-137. doi:10.1038/nature13638

42. Toso A, Revandkar A, Di Mitri D, et al. Enhancing Chemotherapy Efficacy in *Pten*-Deficient Prostate Tumors by Activating the Senescence-Associated Antitumor Immunity. *Cell Reports*. 2014;9(1):75-89. doi:10.1016/j.celrep.2014.08.044

43. Salam R, Saliou A, Bielle F, et al. Cellular senescence in malignant cells promotes tumor progression in mouse and patient Glioblastoma. *Nat Commun*. 2023;14(1):441. doi:10.1038/s41467-023-36124-9

44. Wei W, Dang Y, Chen G, et al. Comprehensive analysis of senescence-related genes identifies prognostic clusters with distinct characteristics in glioma. *Sci Rep*. 2025;15(1):9540. doi:10.1038/s41598-025-93482-8

45. Tsai JW, Choi JJ, Ouaalam H, et al. Integrated response analysis of pediatric low-grade gliomas during and after targeted therapy treatment. *Neuro-Oncology Advances*. 2023;5(1):vdac182. doi:10.1093/noajnl/vdac182

46. Sigaud R, Albert TK, Hess C, et al. MAPK inhibitor sensitivity scores predict sensitivity driven by the immune infiltration in pediatric low-grade gliomas. *Nat Commun*. 2023;14(1):4533. doi:10.1038/s41467-023-40235-8

47. Skwarska A, Konopleva M. BCL-xL Targeting to Induce Apoptosis and to Eliminate Chemotherapy-Induced Senescent Tumor Cells: From Navitoclax to Platelet-Sparing BCL-xL PROTACs. *Cancer Res*. 2023;83(21):3501-3503. doi:10.1158/0008-5472.CAN-23-2804

48. Sigaud R, Rösch L, Gatzweiler C, et al. The first-in-class ERK inhibitor ulixertinib shows promising activity in mitogen-activated protein kinase (MAPK)-driven pediatric low-grade glioma models. *Neuro Oncol*. 2023;25(3):566-579. doi:10.1093/neuonc/noac183

ACCEPTED MANUSCRIPT

Downloaded from academic.oup.com/neuro-oncology/advance-article/doi/10.1093/neuonc/noag270/9004423 by Imperial College of Science Technology and Medicine user on 02 November 2026

49. Riviere-Cazaux C, Carlstrom LP, Neth BJ, et al. An untapped window of opportunity for glioma: targeting therapy-induced senescence prior to recurrence. *npj Precis Onc*. 2023;7(1):126. doi:10.1038/s41698-023-00476-8

50. Gandhi L, Camidge DR, Ribeiro de Oliveira M, et al. Phase I study of Navitoclax (ABT-263), a novel Bcl-2 family inhibitor, in patients with small-cell lung cancer and other solid tumors. *J Clin Oncol*. 2011;29(7):909-916. doi:10.1200/JCO.2010.31.6208

51. Greenberg EF, Voorbach MJ, Smith A, et al. Navitoclax safety, tolerability, and effect on biomarkers of senescence and neurodegeneration in aged nonhuman primates. *Heliyon*. 2024;10(16):e36483. doi:10.1016/j.heliyon.2024.e36483

52. Corcoran RB, Do KT, Kim JE, et al. Phase I/II Study of Combined BCL-xL and MEK Inhibition with Navitoclax and Trametinib in KRAS or NRAS Mutant Advanced Solid Tumors. *Clinical Cancer Research*. 2024;30(9):1739-1749. doi:10.1158/1078-0432.CCR-23-3135

ACCEPTED MANUSCRIPT

Downloaded from academic.oup.com/neuro-oncology/advance-article/doi/10.1093/neuonc/noag270/9004423 by Imperial College of Science Technology and Medicine user on 02 November 2026

Figure Captions.

Figure 1. Trametinib treatment induces senescence and activates the SASP in BT-40 brain tumours in vivo.

(A) A schematic of the experimental design. BT-40 tumour-bearing NSG mice are treated either with Trametinib or vehicle for 7 days, and analyses are performed at day 7 and day 14 (7 days post -Trametinib withdrawal). (B) Tumour growth is measured by bioluminescence imaging and is shown as mean values for 5 individual animals per group as radiance in photons.second^{-1}.cm^{-2}.steradian^{-1} relative to the radiance at day 1 of treatment. Note that although Trametinib treatments leads to a significant reduction in BLI at day 7, there is a quick rebound growth after treatment discontinuation at day 14. Two-way RM ANOVA Geisser-Greenhouse's correction, Šídák's multiple comparisons test between groups at indicated timepoints are indicated vertically, and differences between timepoints for Trametinib group are indicated horizontally. (C) Double immunofluorescence against Human Nuclear Antigen (HNA – red) and either phosphorylated-ERK1/2, Ki67, or the senescent markers p21, GLB1 or LAMP1 (green). DAPI in blue. Scale bars: 200 µm. (D,E) Quantification of the proportion of HNA positive cells or areas expressing the markers used in (C). Note the overall reduction of PERK1/2 and Ki67 (D) but overall increase in senescent marker expression upon Trametinib treatment (E). Data show mean ± SEM of n = 3 BT-40 tumours per marker. Kruskal-Wallis test, Dunn's post-test; *: p<0.05, **: p<0.01, ***: p<0.001.

Figure 2. Trametinib-induced senescent BT-40 tumours express myeloid-attractant chemokines and cytokines, accompanied by prominent myeloid infiltration.

(A) Double immunofluorescence against Human Nuclear Antigen (HNA – red), the myeloid-attractant chemokines/cytokines CCL2, CXCL10 and IL6 (green) and the microglial/monocyte marker IBA1 (green). DAPI in blue. Scale bars: 200 µm. (B) Quantification of the proportion of HNA positive cells expressing the analysed markers in (A). Note the significant increase in marker expression upon Trametinib treatment. (C) Quantification of the proportion of cells expressing the IBA1 marker from (A). Note the significant increase in IBA1 positive cells expression upon and after Trametinib treatment. Data show mean ± SEM of n = 3 BT-40 tumours per marker. Kruskal-Wallis test, Dunn's post-test; ***: p<0.001.

ACCEPTED MANUSCRIPT

Downloaded from academic.oup.com/neuro-oncology/advance-article/doi/10.1093/neuonc/noag270/9004423 by Imperial College of Science Technology and Medicine user on 02 November 2026

Figure 3. Treatment of BT-40 cells in vitro with Dabrafenib, Trametinib, or Vinblastine induces cellular senescence and activates the SASP.

(A) Diagram of the experimental approach. Cultured BT-40 cells are treated with either of the drugs at day 0 for 24h, followed by a wash-out period of 6 days in the absence of drug, and analysed at day 7 both molecularly (RNA-seq) and by immunocytochemistry. (B) SA-β-Gal staining indicating the increase of blue-stained cells after drug treatment compared with vehicle-treated control. Kruskal-Wallis test, Dunn's post-test; *: $p<0.05$, **: $p<0.01$. (C) $p21^{Cip1}$ immunostaining showing the accumulation of nuclear fluorescence signal in the drug-treated cells compare with vehicle controls. (D) Volcano plot of differentially expressed genes comparing proliferative and drug-treated BT-40 cells. Thresholds used: p-values < 0.05 and log2 FoldChange > 1. (E) Normalized enrichment scores (NES) from GSEA showing decreased proliferation-associated genesets and increased senescence and SASP-related genesets for each of the treatment (Dabrafenib, Trametinib and Vinblastine) compared with vehicle control cells. The crossed dots represent the NES integrating the three treated conditions versus the vehicle control. (F) Immunofluorescence staining of IL1B and CCL2 (red) at day 7 in vehicle-treated and drug-treated BT-40 cultured cells. DAPI in blue. Scale bars: 100 µm. (G) Heat maps showing the relative expression of selected SASP factors in vehicle-treated and drug-treated BT-40 cells. Note that there are specific differences between treatments. IL: Interleukin, GF: Growth factors, Pt^{ases}: matrix proteases. n=6 biological replicates for vehicle-treated BT-40, n=3 biological replicates for dabrafenib, trametinib and vinblastine-treated BT-40.

Figure 4. Treatment-induced senescent BT-40 cells are selectively vulnerable to Bcl-xL inhibition.

(A) Schematic of the experimental design. Drug treatment is carried out for one day, followed by a wash-out period of 6 days in the absence of drug. At day 7, control proliferative and treatment-induced BT-40 cells are cultured in the presence of senolytics for 3 days. (B) Heatmap showing the drug sensitivity score (DSS) of several inhibitors of the Bcl-2 family of anti-apoptotic proteins and known senolytics used on cells pre-treated with vehicle, Dabrafenib, Trametinib or Vinblastine. Note that the highest DDSs are observed with Navitoclax, A-1155463, A-1331852 and Obatoclax, which all inhibit Bcl-xL, while the weak Bcl-xL inhibitor, but strong Bcl-2 inhibitor Venetoclax or the senolytics (Piperlongumine and Digoxin) show lower DSSs. (C) Dose response curves of Navitoclax on BT-40 cells pre-treated with either Dabrafenib, Trametinib, Vinblastine or vehicle control. Note

ACCEPTED MANUSCRIPT

Downloaded from academic.oup.com/neuro-oncology/advance-article/doi/10.1093/neuonc/noag270/9004423 by Imperial College of Science Technology and Medicine user on 02 November 2026

that the IC50 values are lower in treatment-induced senescent cells than in proliferative BT-40 cells. (D) Navitoclax sensitivity (top: Selt_BT308.UP) and resistance (Marczyk_Navitoclax resistance) scores inferred from ssGSEA analysis of RNA sequencing data of drug-treated and vehicle controls. (E) Graph showing Caspase 3/7 enzymatic activity of treatment-induced senescent or proliferative, vehicle control BT-40 cells and cultured in the presence of 0.1uM or 1mM Navitoclax as shown in (A). Note the significant increase in senescent cells relative to proliferative control cells. AU Normalized activity by cell numbers. Kruskal-Wallis test, Dunn's post-test; ***: p<0.001.

Figure 5. Combination therapy with Trametinib and Navitoclax demonstrates significant anti-tumour activity and extends survival in BT-40 tumour-bearing mice.

(A) Schematic of the preclinical experimental design. Upon engraftment of BT-40 cells, tumour-bearing mice were split into 4 experimental groups: (i) vehicle treated for 3 weeks; ii) Navitoclax treated for 2 weeks (weeks 2 and 3); (iii) Trametinib treated for 3 weeks; (iv) Combination group in which mice were treated with Trametinib for 3 weeks and Navitoclax on weeks 2 and 3. (B) Kaplan-Meier estimator plots showing the probability of survival of the mice in the 4 different groups. Pairwise comparisons using Log-Rank test: Combi. vs. Veh.: p=0.0001 ; Combi. vs. Nav.: p= 0.0005 ; Combi. vs. Tram.: p= 0.0008 ; Tram. vs. Nav.: p= 0.0028 ; Tram. vs. Veh.: p= 0.0020. (C) Average BLI fold-change in the 4 experimental groups relative to the average BLI at day 1 of treatment. Tukey's multiple comparisons test at day 15: Tram. vs. Nav.&Veh.: p <0.0001 ; Combi. vs. Nav.&Veh.: p <0.0001. Tukey's multiple comparisons test at day 35: Tram. vs. Combi.: p=0.0028. (D) BLI fold-change for each individual mice in the 4 experimental groups relative to the BLI at day 1 of treatment. (E) Double immunofluorescence against Human Nuclear Antigen (HNA - red) and the proliferation marker Ki67, the apoptosis marker cleaved-caspase-3 (CC3), or the senescent marker GLB1 (green). DAPI in blue. Scale bars: 200 µm. (F) Quantification of the proportion of HNA positive cells expressing Ki67 and the percentage of tumour area positive for CC3 and GLB1 analysed in (E). Data show mean ± SEM of n = 3 BT-40 tumours per marker. Kruskal-Wallis test, Dunn's post-test; *: p<0.05, **: p<0.01, ***: p<0.001.

Figure 6. Combination therapy with Trametinib and Navitoclax reduces myeloid infiltration in BT-40 tumours in vivo.

ACCEPTED MANUSCRIPT

Downloaded from academic.oup.com/neuro-oncology/advance-article/doi/10.1093/neuonc/noag270/9004423 by Imperial College of Science Technology and Medicine user on 02 November 2026

(A) Double immunofluorescence against Human Nuclear Antigen (HNA – red) and microglial/monocyte markers (IBA1 and TIM3 - green). DAPI in blue. Scale bars: 200 µm. (B) Quantification of the proportion of DAPI positive cells expressing the stated markers from (A). Kruskal-Wallis test, Dunn's post-test; *: $p<0.05$, **: $p<0.01$, ***: $p<0.001$. (C) Schematic model summarizing the responses of BT-40 cells to Trametinib or Trametinib plus Navitoclax treatment in BT-40 tumour-bearing mice. Trametinib induces robust senescence and activates the SASP, including myeloid-attractant factors (e.g., IL6, CCL2, CXCL10). Upon Trametinib withdrawal, BT-40 cells resume proliferation and myeloid infiltration increases. In contrast, combination therapy with Trametinib and Navitoclax selectively ablates senescent BT-40 cells, modulates the SASP, reduces myeloid infiltration, and promotes tumour clearance. Created in BioRender. https://BioRender.com/3eiatvn

ACCEPTED MANUSCRIPT

Downloaded from academic.oup.com/neuro-oncology/advance-article/doi/10.1093/neuonc/noag270/9004423 by Imperial College of Science Technology and Medicine user on 02 November 2026

Standard treatment against paediatric BRAF-V600E glioma promotes senescence and sensitizes tumours to BCL-xL inhibition

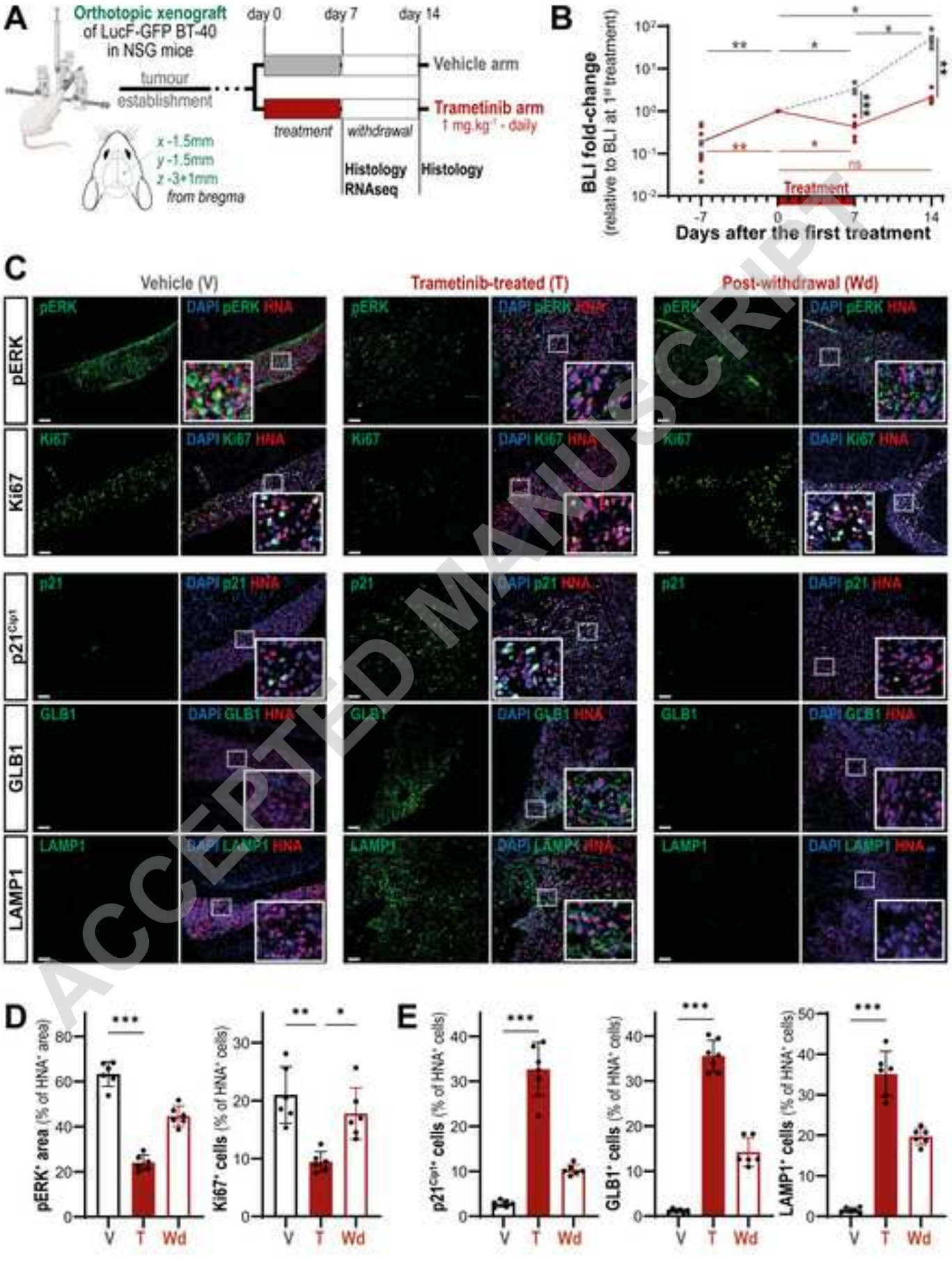
Lay summary

Children with BRAF-V600E gliomas can respond well to treatment, but tumours may return after therapy stops. We reveal that standard treatment can push some tumour cells into a state called cellular senescence, in which they stop growing but remain alive. These senescent cells release signals that alter the tumour environment and may contribute to tumour recurrence. Importantly, we found that senescent tumour cells can be eliminated using drugs called senolytics. We show that combining standard treatment with a senolytic approach prevents tumour regrowth and significantly improves survival in mouse models.

ACCEPTED MANUSCRIPT

Downloaded from academic.oup.com/neuro-oncology/advance-article/doi/10.1093/neuonc/noag270/9004423 by Imperial College of Science Technology and Medicine user on 02 November 2026

Click here to access/download;Figure;Figure_1.tif

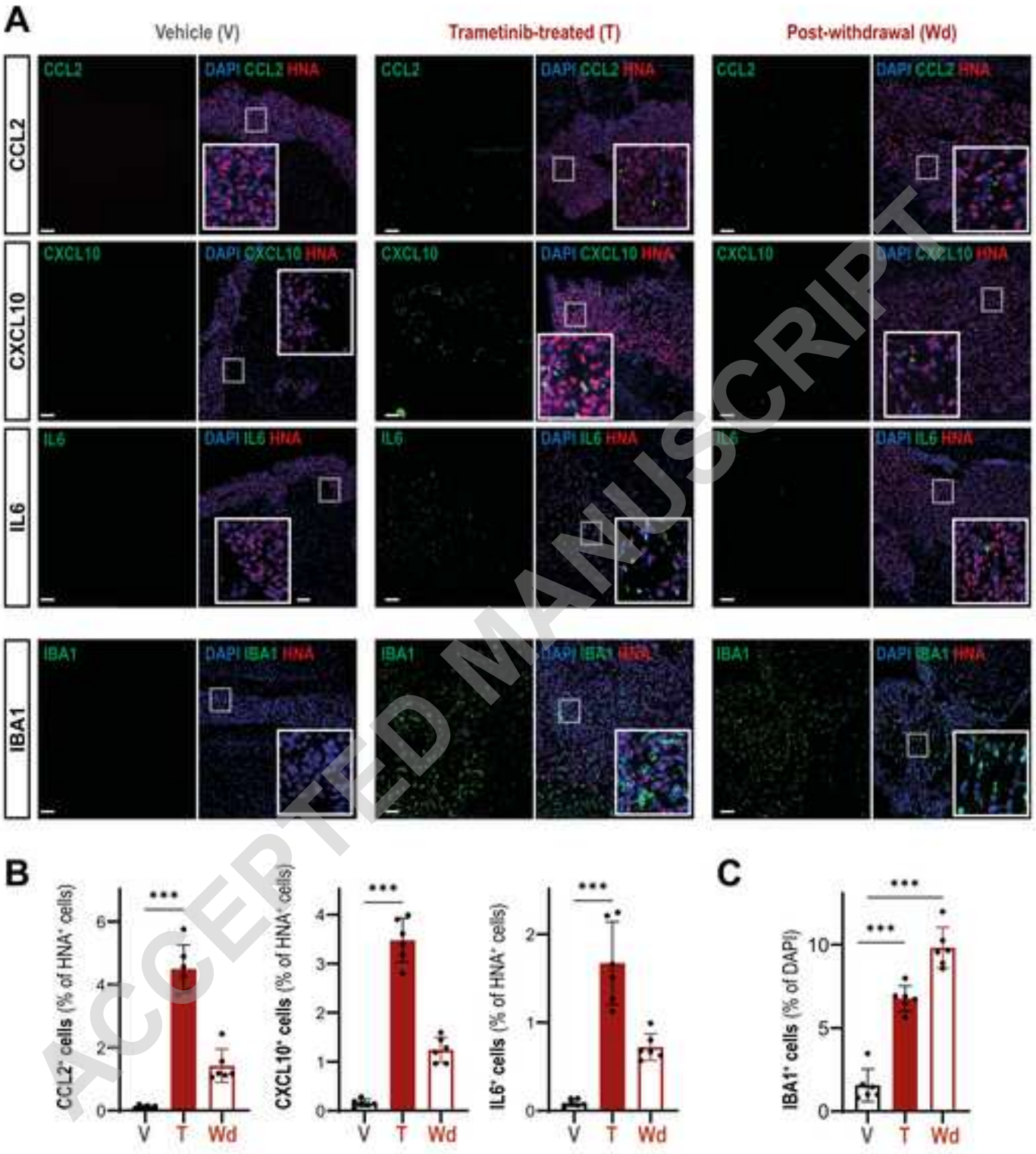


ACCEPTED MANUSCRIPT

Downloaded from academic.oup.com/neuro-oncology/advance-article/doi/10.1093/neuonc/noag270/9004423 by Imperial College of Science Technology and Medicine user on 02 November 2026

Figure 2

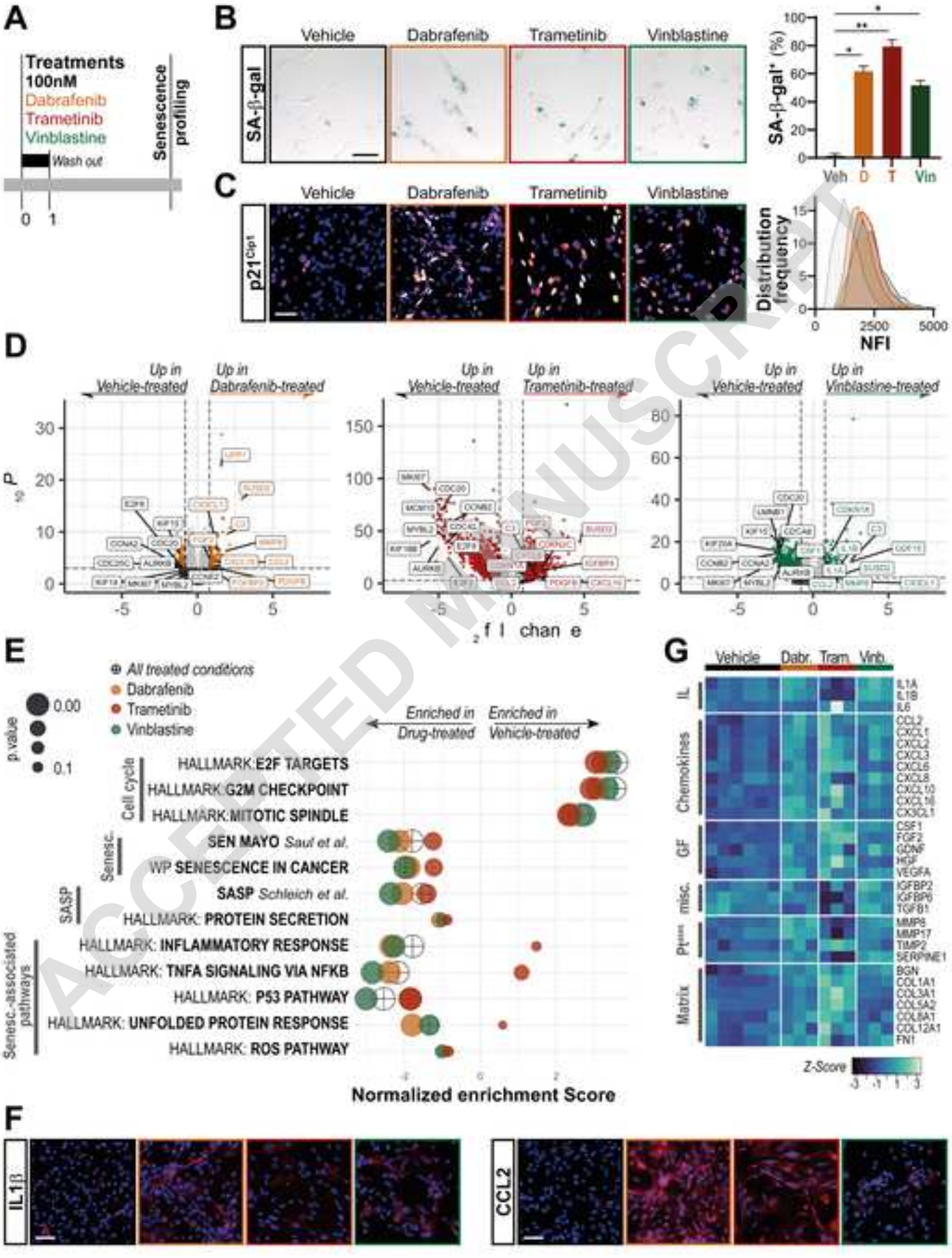
Click here to access/download;Figure;Figure_2.tif



ACCEPTED MANUSCRIPT

Downloaded from academic.oup.com/neuro-oncology/advance-article/doi/10.1093/neuonc/noag270/9004423 by Imperial College of Science Technology and Medicine user on 02 November 2026

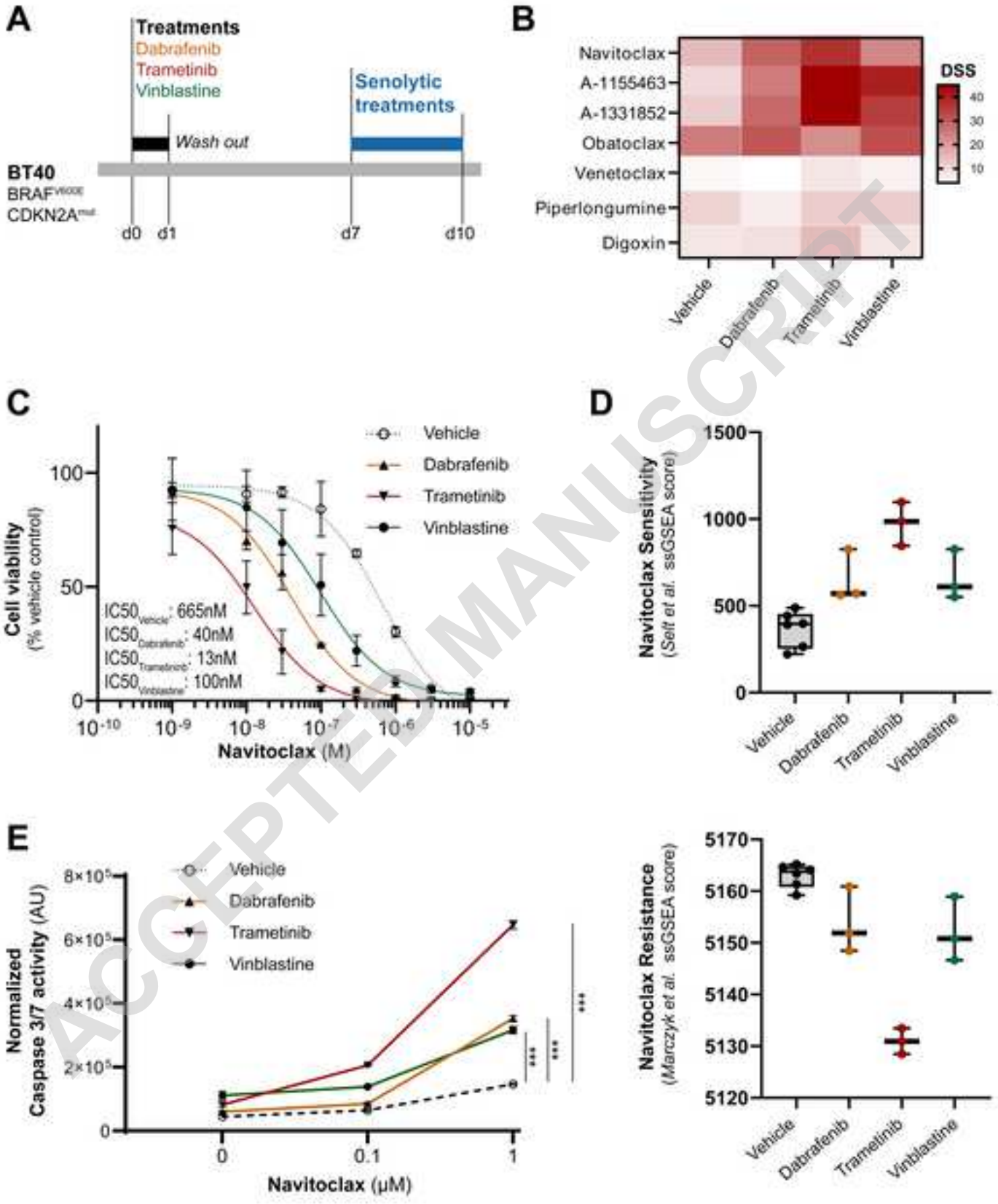
Click here to access/download;Figure;Figure_3.tif



ACCEPTED MANUSCRIPT

Downloaded from academic.oup.com/neuro-oncology/advance-article/doi/10.1093/neuonc/noag270/9004423 by Imperial College of Science Technology and Medicine user on 02 November 2026

Click here to access/download;Figure;Figure_4.tif

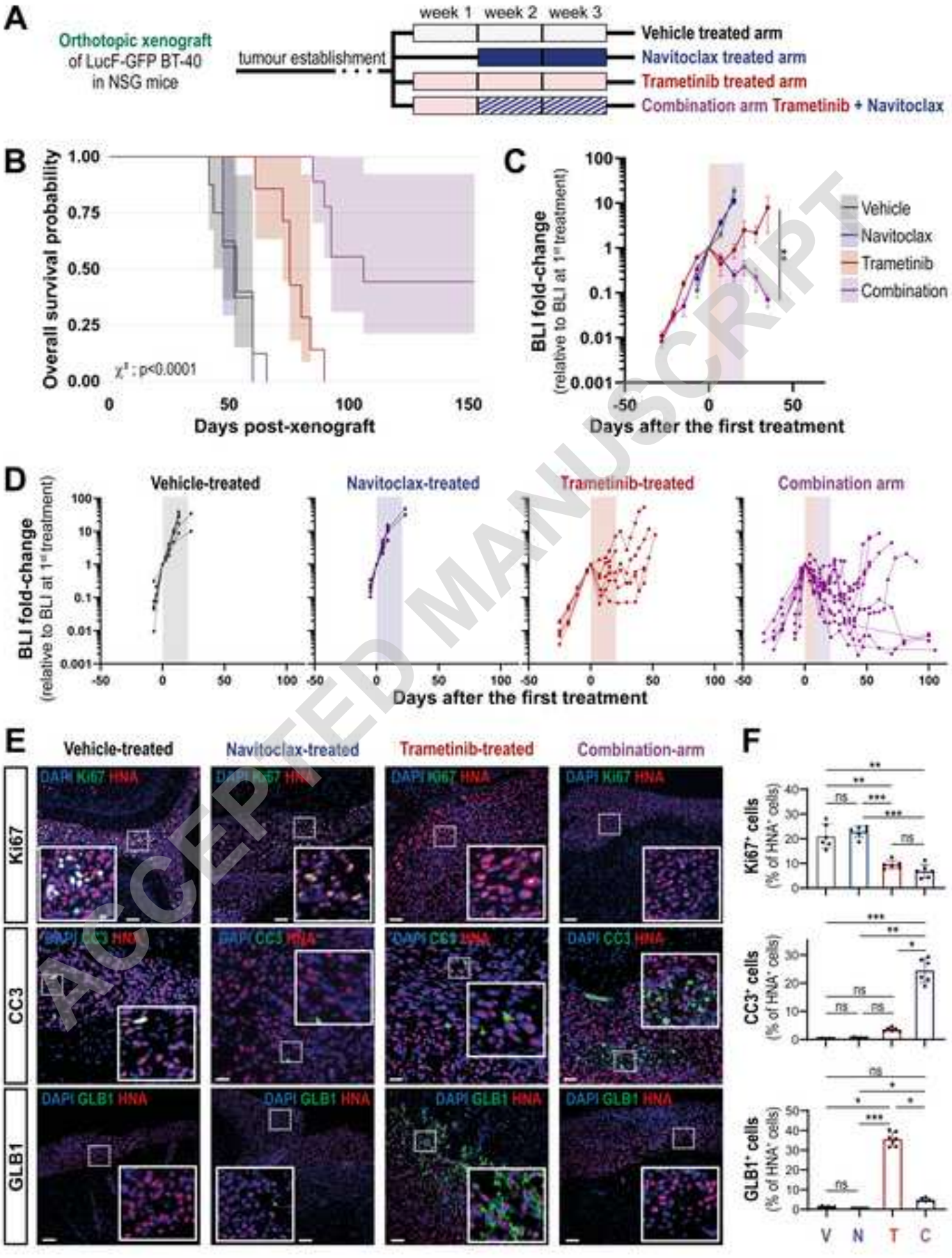


ACCEPTED MANUSCRIPT

Downloaded from academic.oup.com/neuro-oncology/advance-article/doi/10.1093/neuonc/noag270/9004423 by Imperial College of Science Technology and Medicine user on 02 November 2026

Figure 5

Click here to access/download;Figure;Figure_5.tif

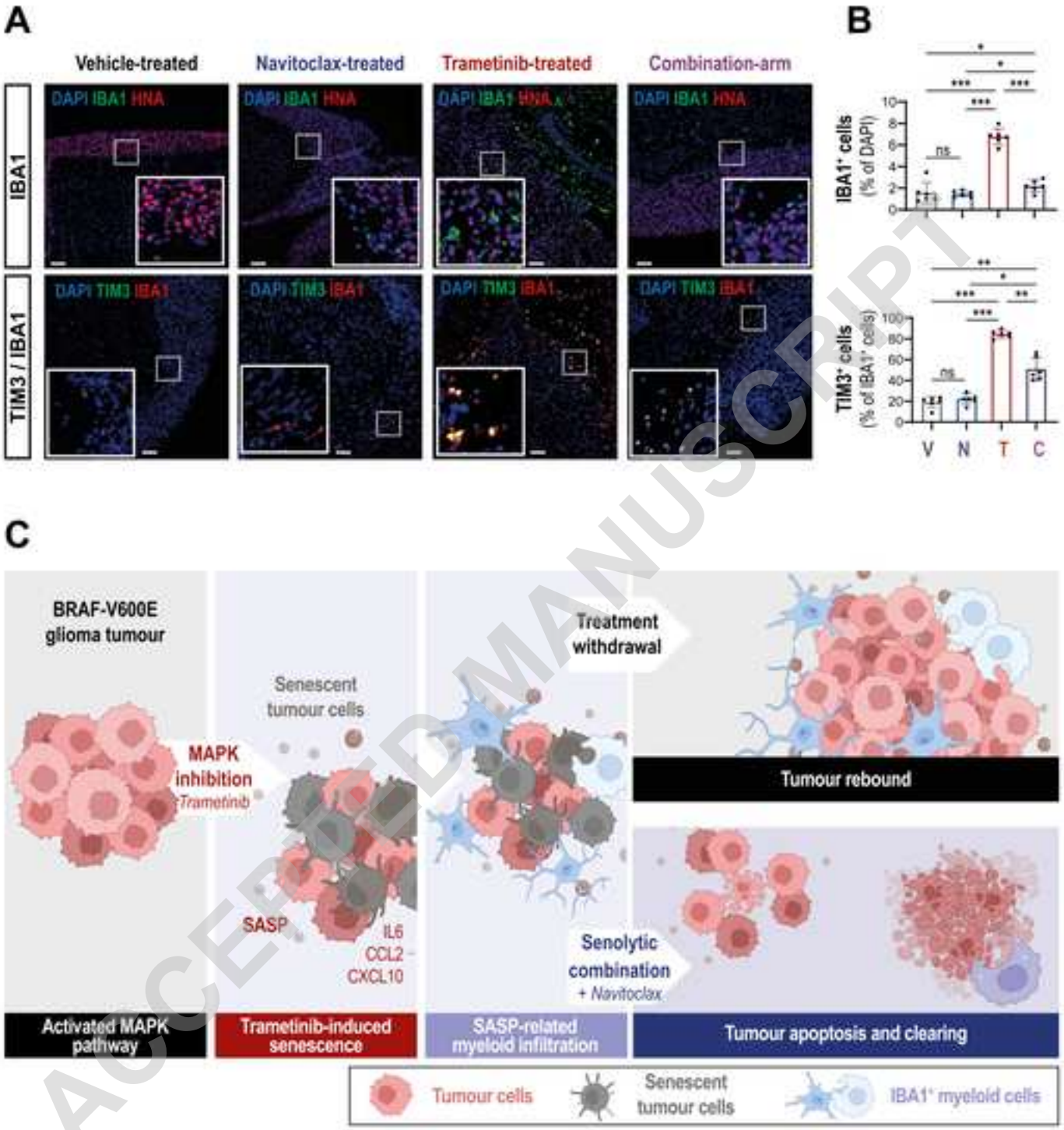


ACCEPTED MANUSCRIPT

Downloaded from academic.oup.com/neuro-oncology/advance-article/doi/10.1093/neuonc/noag270/9004423 by Imperial College of Science Technology and Medicine user on 02 November 2026

Figure 6

Click here to access/download;Figure;Figure_6.tif



ACCEPTED MANUSCRIPT

Downloaded from academic.oup.com/neuro-oncology/advance-article/doi/10.1093/neuonc/noag270/9004423 by Imperial College of Science Technology and Medicine user on 02 November 2026

Data Integrity Supplement for Manuscript N-O-D-26-00091R1

Table of author attribution for display items in manuscript

Display Item	Created by Author(s):
Figure 1A-B	Romain GUIHO
Figure 1C-E	Hiba HAMDI, Romain GUIHO
Figure 2	Hiba HAMDI, Romain GUIHO
Figure 3	Romain GUIHO
Figure 4A-C,E	Romain GUIHO
Figure 4D	Romain SIGAUD, Romain GUIHO
Figure 5A-D	Romain GUIHO
Figure 5E-F	Hiba HAMDI, Romain GUIHO
Figure 6A-B	Hiba HAMDI, Romain GUIHO
Figure 6C	Romain GUIHO
Suppl Figure S1	Romain GUIHO
Suppl Figure S2	Romain GUIHO
Suppl Figure S3	Romain GUIHO
Suppl Figure S4	Romain GUIHO
Suppl Figure S5	Timoty H. CHANG
Suppl Figure S6	Timoty H. CHANG
Suppl Figure S7	Romain GUIHO, Sophie BLISS
Suppl Figure S8	Romain GUIHO
Suppl Figure S9	Hiba HAMDI, Romain GUIHO
Suppl Table S1	Romain GUIHO, Ashley VARDON
Suppl Table S2	Hiba HAMDI, Romain GUIHO
Suppl Table S3-4-5-6	Romain GUIHO

ACCEPTED MANUSCRIPT

Downloaded from academic.oup.com/neuro-oncology/advance-article/doi/10.1093/neuonc/noag270/9004423 by Imperial College of Science Technology and Medicine user on 02 November 2026

Fig1C

Entire fields of FFPE showing immunofluorescence for pERK, Ki67, p21^{Cip1}, GLB1 and LAMP1. Human Nuclear Antigen was used for identification of human cells, pseudocolorized in red with Zen (Zeiss). Counterstained with DAPI (blue).
For staining channels, LUT are fixed at {min=26329; max=62237} for pERK, {min=2080; max=14466} for Ki67, {min=9646; max=13231} for p21^{Cip1}, {min=11898; max=22518} for GLB1 and {min=2473; max=8237} for LAMP1, 16-bit greyscale pictures are pseudocolorized in green with Zen.

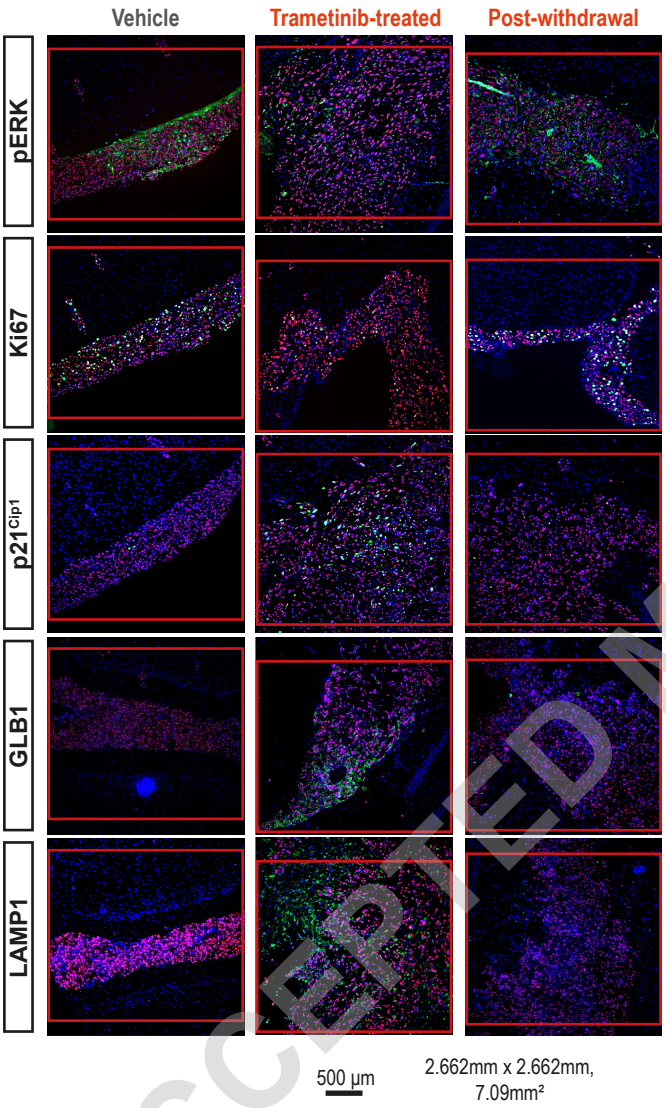
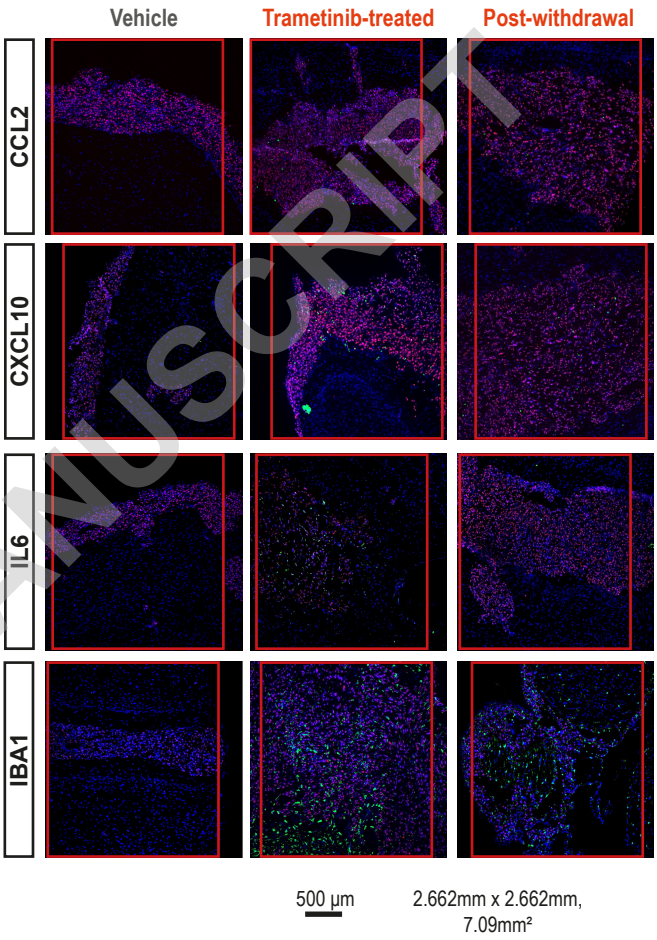


Fig2A

Entire fields of FFPE showing immunofluorescence for CCL2, CXCL10, IL6 and IBA1. Human Nuclear Antigen was used for identification of human cells, pseudocolorized in red with Zen (Zeiss). Counterstained with DAPI (blue).
For staining channels, LUT are fixed at {min=6876; max=9481} for CCL2, {min=5103; max=6251} for CXCL10, {min=9035; max=12698} for IL6, and {min=9893; max=20329} for IBA1, 16-bit greyscale pictures are pseudocolorized in green with Zen.



ACCEPTED MANUSCRIPT

Downloaded from academic.oup.com/neuro-oncology/advance-article/doi/10.1093/neuonc/noag270/9004423 by Imperial College of Science Technology and Medicine user on 02 November 2026

Fig3B

Entire fields of cells showing SA-beta-Gal colorimetric staining in bright-field stereoscopy (Leica software).
After white balance, the saturation of the images was enhanced by 20%.

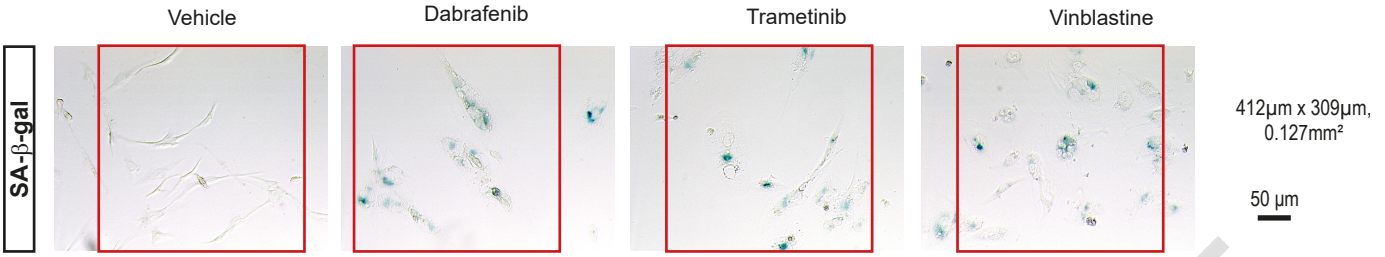


Fig3C

Entire fields of cells showing immunofluorescence p21 staining. Counterstained with DAPI (blue).
For staining channel, LUT are fixed at {min=0;max=87/255}, 8bits greyscale pictures are pseudocolorized with Fiji «Fire» preset.

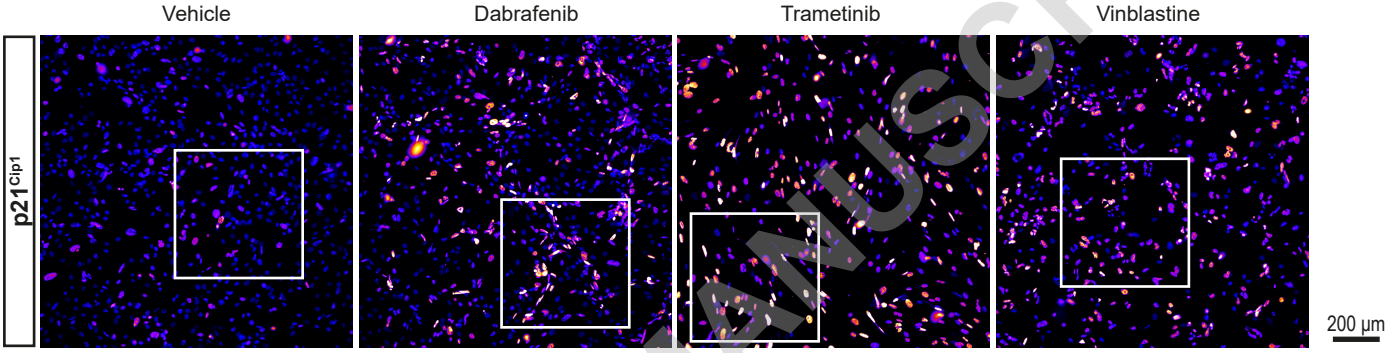
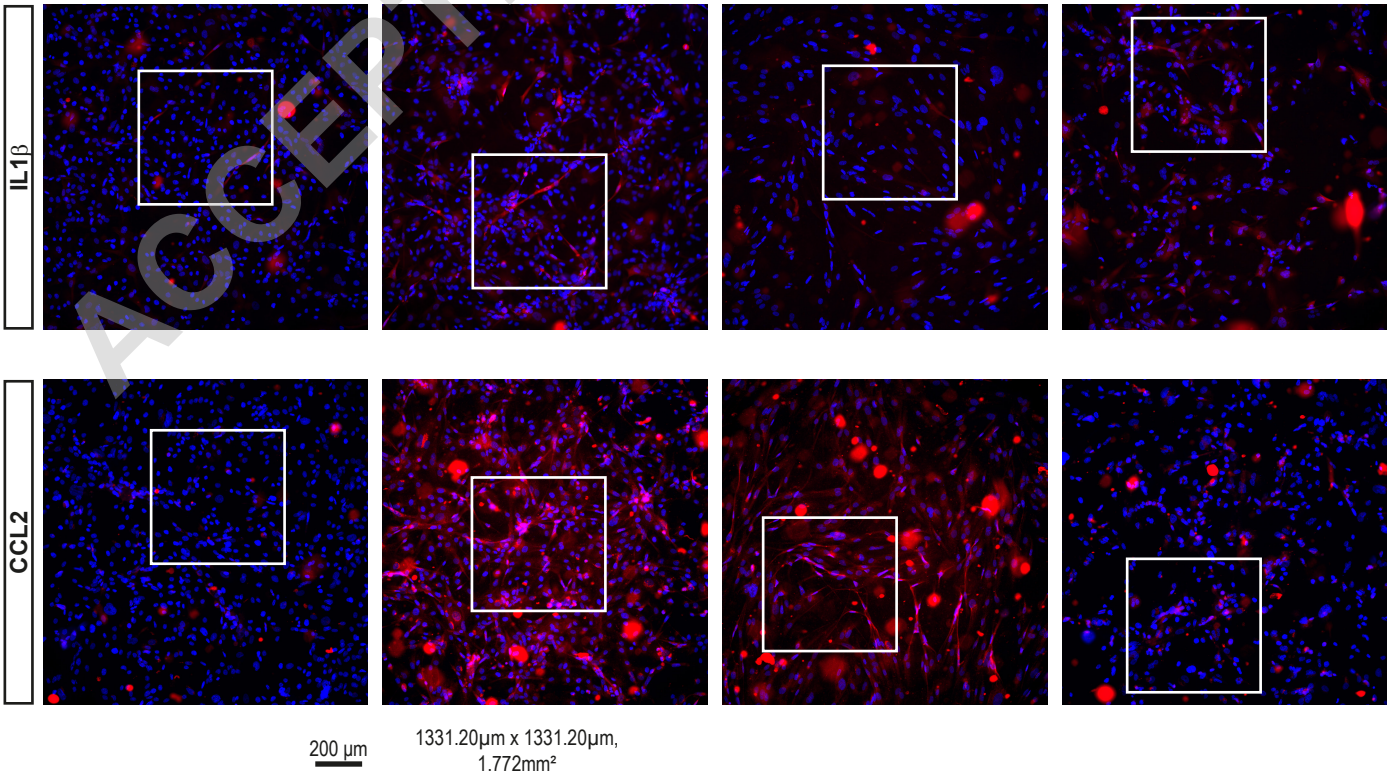


Fig3F

Entire fields of cells showing immunofluorescence IL1beta and CCL2 stainings. Counterstaned with DAPI pseudocolorized in blue with Fiji.
For staining channel, LUT are fixed at {min=3;max=107/255} for IL1B and {min=11;max=53/255} for CCL2, 8bits greyscale pictures are pseudocolorized in red with Fiji.



ACCEPTED MANUSCRIPT

Downloaded from academic.oup.com/neuro-oncology/advance-article/doi/10.1093/neuonc/noag270/9004423 by Imperial College of Science Technology and Medicine user on 02 November 2026

Fig5E

Entire fields of FFPE showing immunofluorescence for Ki67, CC3 and GLB1. Human Nuclear Antigen was used for identification of human cells, pseudocolorized in red with Zen (Zeiss). Counterstained with DAPI (blue).
For staining channels, LUT are fixed at {min=2019; max=14322} for Ki67, {min=9618; max= 22527} for CC3, and {min=12504; max=43688} for GLB1, 16-bit greyscale pictures are pseudocolorized in green with Zen.

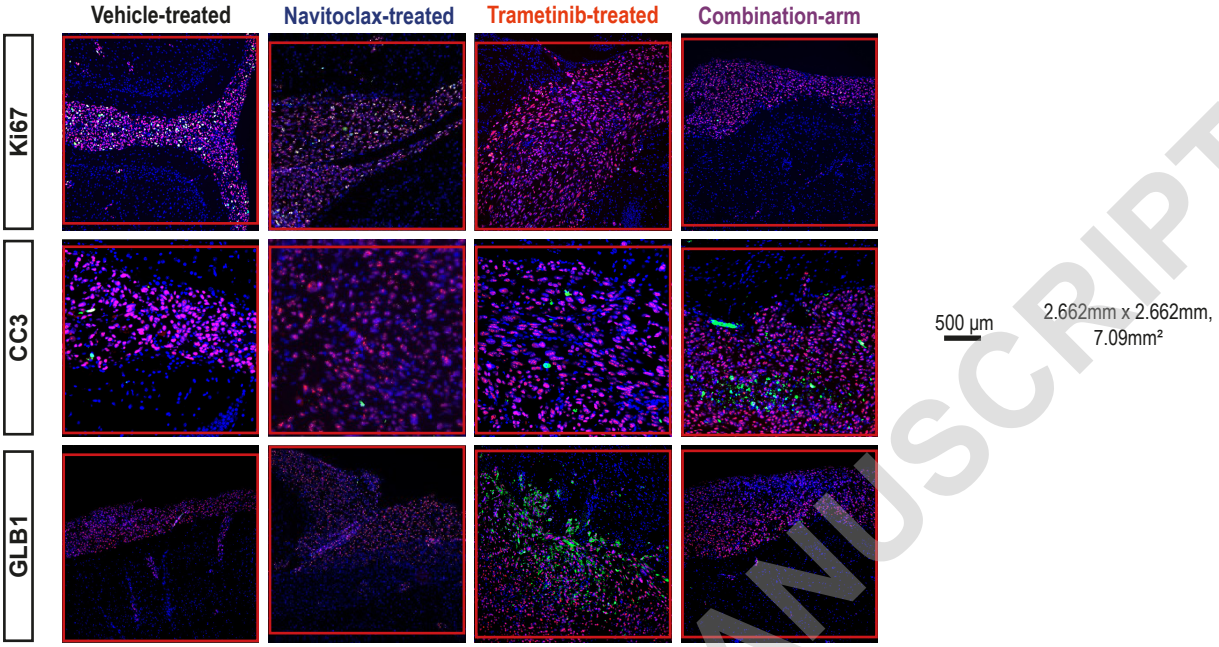
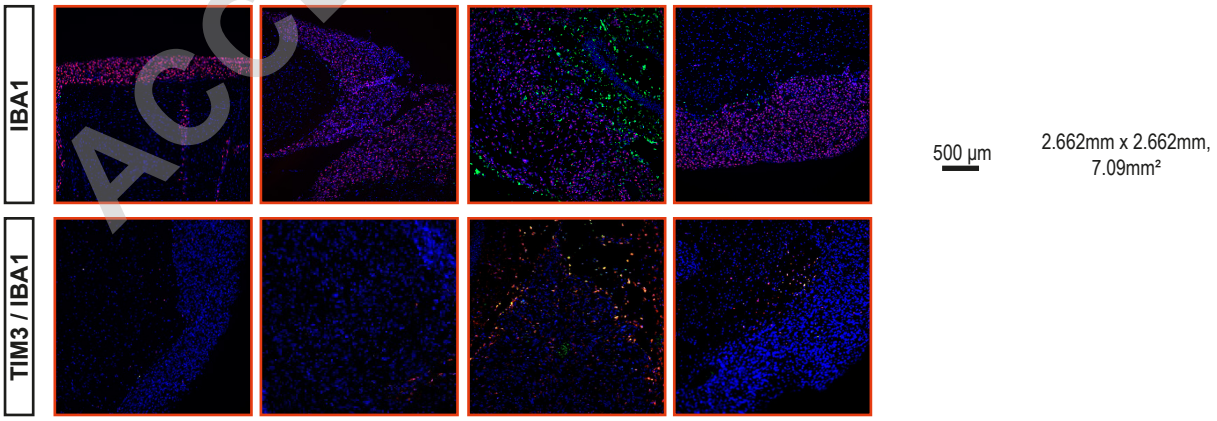


Fig6A

Entire fields of FFPE showing immunofluorescence for IBA1 and IBA1/TIM3.
For IBA1 alone, Human Nuclear Antigen was used for identification of human cells, pseudocolorized in red with Zen (Zeiss). Counterstained with DAPI (blue). LUT are fixed at {min= 13283; max= 32505} for IBA1

For IBA1/TIM3, IBA1 staining is pseudocolorized in red with Zen, 16bit LUT at {min=2485; max=14961} and TIM3 is pseudocolorized in green, 16-bit LUT at {min=2485; max=14961}. Counterstained with DAPI (blue).

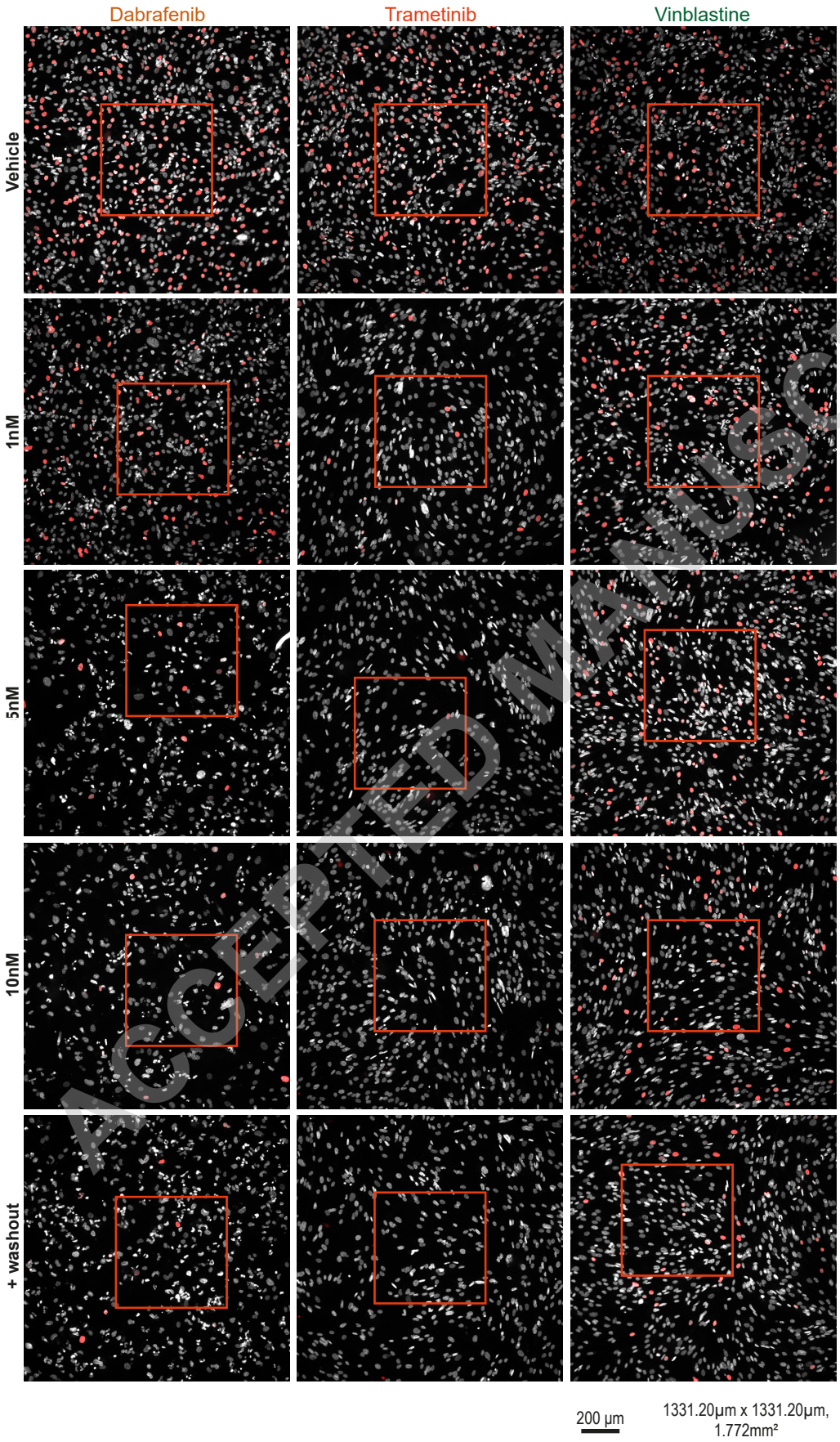


ACCEPTED MANUSCRIPT

Downloaded from academic.oup.com/neuro-oncology/advance-article/doi/10.1093/neuonc/noag270/9004423 by Imperial College of Science Technology and Medicine user on 02 November 2026

Fig. S2

Entire fields of cells showing EdU incorporation performed using Click-iT EdU 488 Cell Proliferation Kit (Invitrogen).
Counterstaned with DAPI pseudocolorized in light grey.
For EdU channel, LUT are fixed at {min=2,000;max=45,000/65,535}, 16-bit greyscale pictures are pseudocolorized in red with ZEISS Zen software.

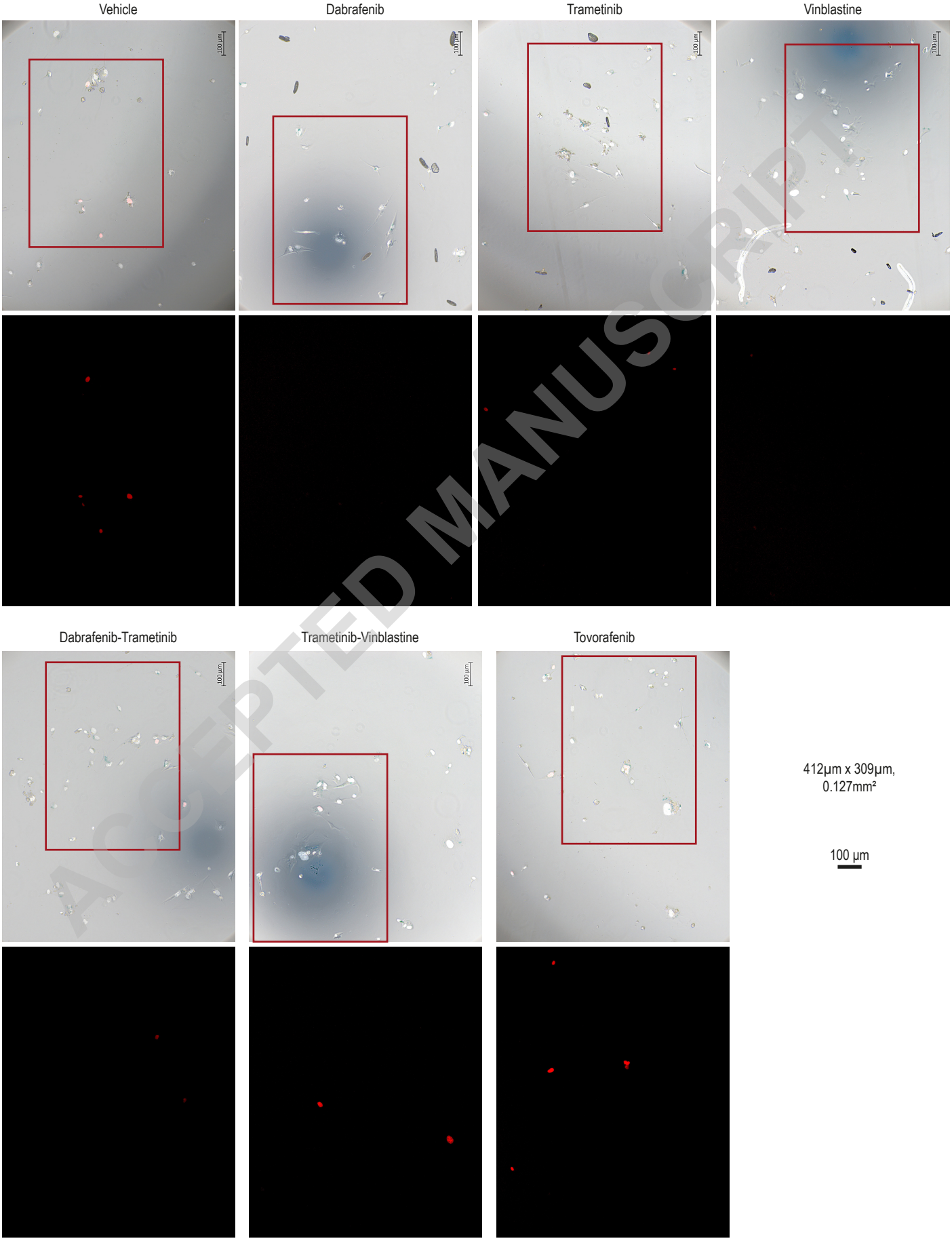


ACCEPTED MANUSCRIPT

Downloaded from academic.oup.com/neuro-oncology/advance-article/doi/10.1093/neuonc/noag270/9004423 by Imperial College of Science Technology and Medicine user on 02 November 2026

Fig. S3B,E

Entire fields of cells showing SA-beta-Gal colorimetric staining in bright-field stereoscopy (Zen software). After white balance, the saturation of the images was enhanced by 10%.
EdU incorporation staining on the same cells was performed using Click-iT EdU 488 Cell Proliferation Kit (Invitrogen). Counterstaned with DAPI pseudocolorized in dark grey. For EdU channel, LUT are fixed at {min=2,000;max=5,000/65,535}, 16-bit greyscale pictures are pseudocolorized in red with ZEISS Zen software.



ACCEPTED MANUSCRIPT

Downloaded from academic.oup.com/neuro-oncology/advance-article/doi/10.1093/neuonc/noag270/9004423 by Imperial College of Science Technology and Medicine user on 02 November 2026

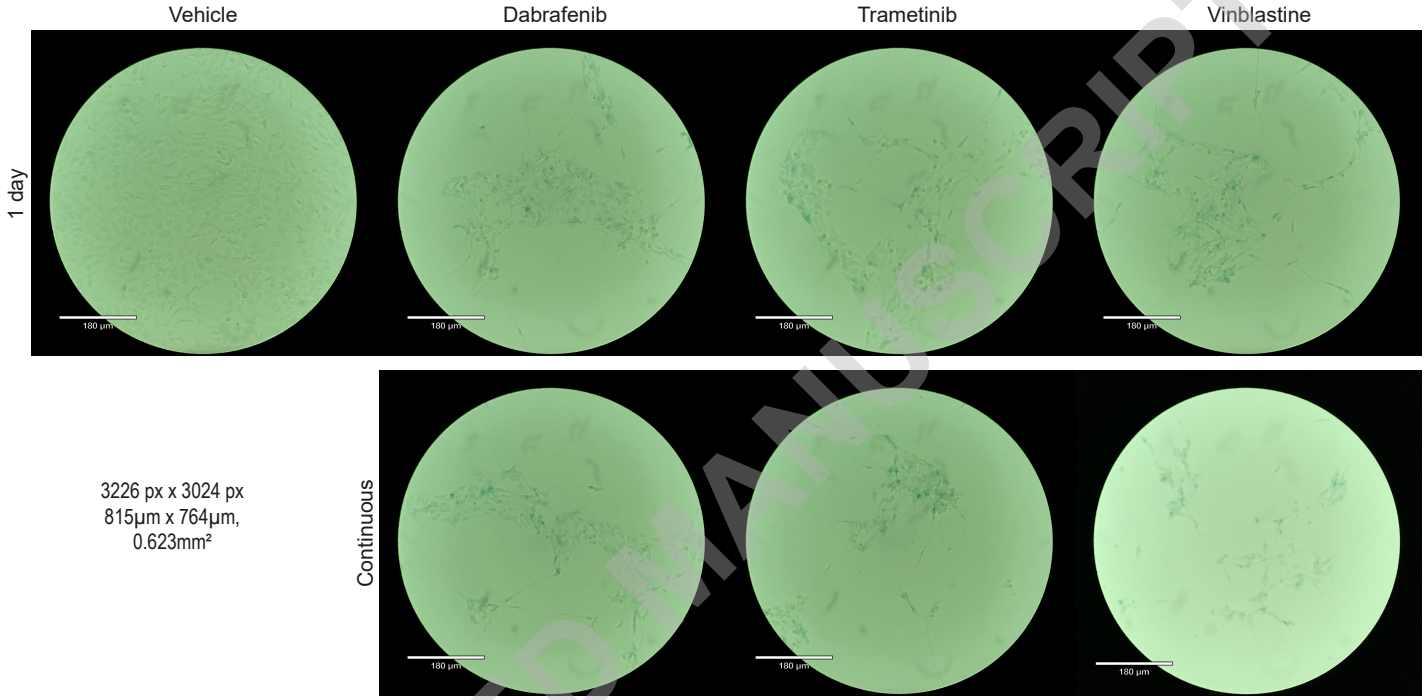
Fig. S6B

Original uncropped brightfield images showing SA-β-gal staining are provided as individual files. The images labeled “Raw” represent the original uncropped images.

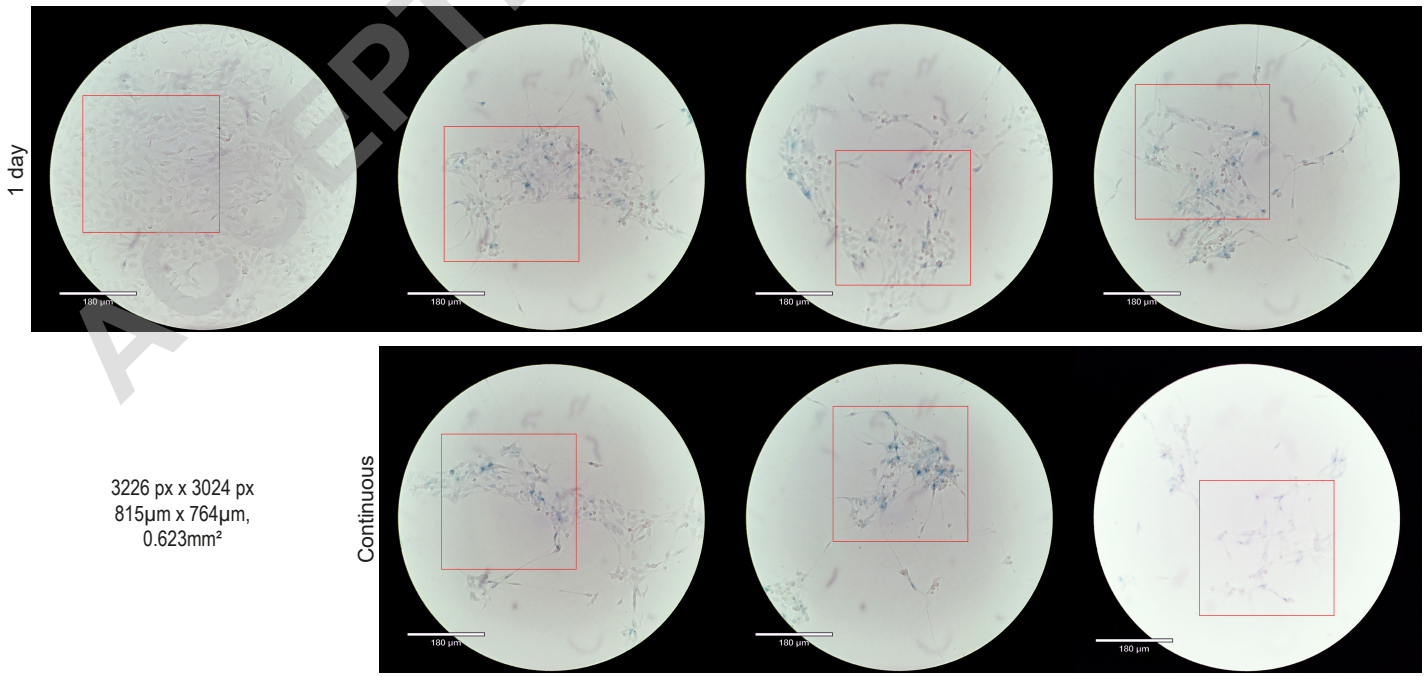
For figure preparation, the raw images were opened in Adobe Photoshop. All images were treated in the following manner: levels were adjusted using Image > Adjustments > Levels, with the gray point sampler used to set the gray point by selecting a location closest to the center of the image that did not contain a cell. Brightness was then adjusted to +20 and contrast to +100. These settings produced the images labeled “adjusted uncropped”.

A red box was added to the adjusted uncropped image to indicate the region selected for the final figure panel. The final figure image was generated by cropping this boxed region. No LUT was applied.

Raw images



Adjusted uncropped

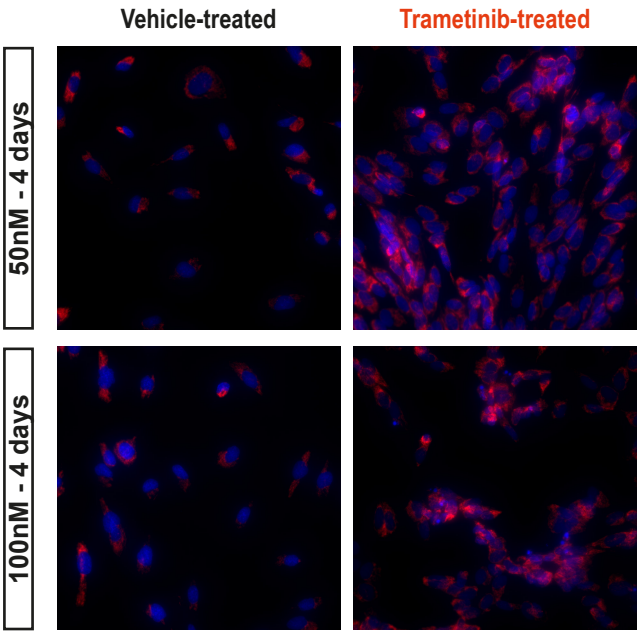


ACCEPTED MANUSCRIPT

Downloaded from academic.oup.com/neuro-oncology/advance-article/doi/10.1093/neuonc/noag270/9004423 by Imperial College of Science Technology and Medicine user on 02 November 2026

Fig. S7G

Entire field of view (x40 magnification) showing immunofluorescent BCL-XL staining (red). Counterstained with DAPI in blue. Images were pseudo colorized using FIJI. Images were acquired using the ImageXpress HCS.ai High-Content Screening System.
50nm and untreated images: LUT were fixed at (min = 1951; max = 10574).
100nM and untreated images: LUT were fixed at (min=1931; max=10738)



ACCEPTED MANUSCRIPT

Downloaded from academic.oup.com/neuro-oncology/advance-article/doi/10.1093/neuonc/noag270/9004423 by Imperial College of Science Technology and Medicine user on 02 November 2026

Fig. S9A

Entire fields of FFPE showing immunofluorescence for p21^{Cip1} and LAMP1. Human Nuclear Antigen was used for identification of human cells, pseudocolorized in red with Zen (Zeiss). Counterstained with DAPI (blue).
For staining channels, LUT are fixed at {min=9915; max=12551} for p21^{Cip1} and {min=14325; max= 23492} for LAMP1, 16-bit greyscale pictures are pseudocolorized in green with Zen.

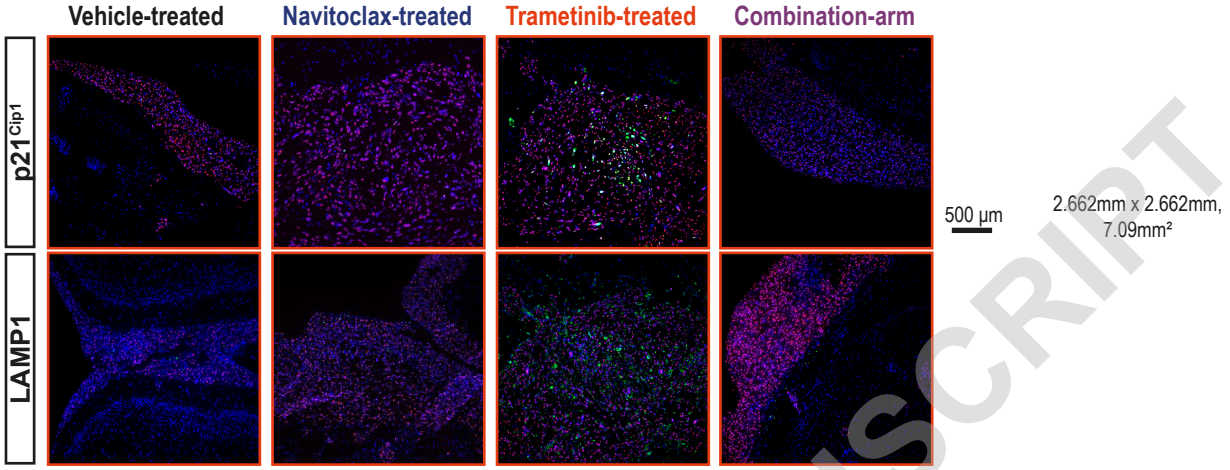
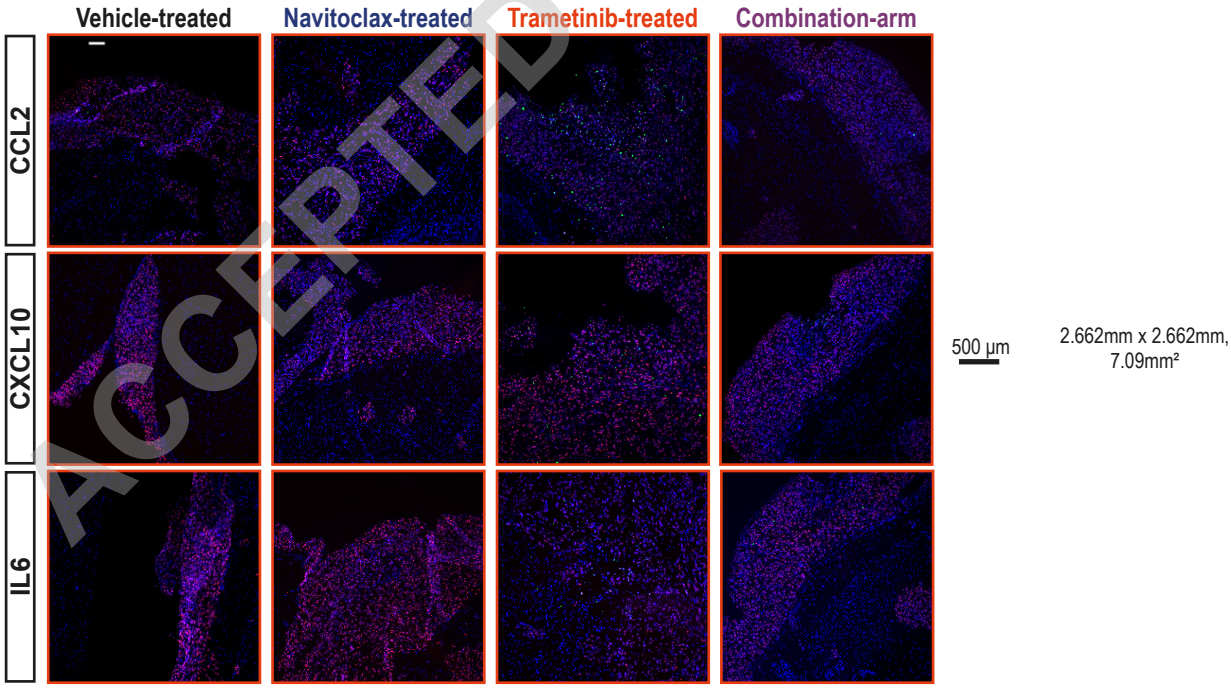


Fig. S9C

Entire fields of FFPE showing immunofluorescence for CCL2, CXCL10 and IL6. Human Nuclear Antigen was used for identification of human cells, pseudocolorized in red with Zen (Zeiss). Counterstained with DAPI (blue).
For staining channels, LUT are fixed at {min=8852; max=23516} for CCL2, {min=5606; max= 8866} for CXCL10 and {min=7189; max= 12190} for IL6, 16-bit greyscale pictures are pseudocolorized in green with Zen.



ACCEPTED MANUSCRIPT

Downloaded from academic.oup.com/neuro-oncology/advance-article/doi/10.1093/neuonc/noag270/9004423 by Imperial College of Science Technology and Medicine user on 02 November 2026